



UNIVERSITÉ
LIBRE
DE BRUXELLES



VRIJE
UNIVERSITEIT
BRUSSEL

Design of a didactic centrifugal ring positioner

Xavier JORDENS



Master thesis submitted under the supervision of
Prof. Michel Kinnaert
the co-supervision of
Laurent Catoire

in order to be awarded the Degree of
Master of Science in Chemical and Materials
Engineering
major in Process Technology

Academic year
2019 – 2020

Title: Design of a didactic centrifugal ring positioner

Author: Xavier JORDENS

Master of Science in Chemical and Materials Engineering – major in Process Technology

Academic year: 2019 – 2020

Abstract

Within the years, control engineering has constantly evolved and has become present in multiple areas. The evolution of control theory is closely linked to the ability for control engineering students and researchers to perform practical experiments. This master thesis aims at designing, building and controlling an unstable control benchmark yet poorly reported in the literature, called centrifugal ring positioner. This system is meant to be used as an experimental device for control engineering students. The main control requirement of the centrifugal ring positioner is defined as ring position setpoint tracking. The rotation of the system is achieved by a DC gearmotor driven by a driver receiving analog signal from an Arduino DUE microcontroller. Most of the pieces of the system have been 3D-printed using Poly-Lactic Acid (PLA) as printing material. The motor angular velocity is measured with an incremental encoder while an optical infrared sensor is used to monitor the ring position. The centrifugal ring positioner is controlled via a cascade control strategy. The inner loop, consisting of the control of the motor angular velocity, is controlled by a P controller. Two different controllers, a PID and a PD, are designed to control the outer loop, which output consists of the ring position. The PD controller is considered to obtain a closed-loop system with a higher phase margin. Both controllers fulfill the requirement in simulation as well as on the real device. The PID actually shows better control results than the PD controller since its integrating part allows to strongly limit the offset with respect to the position setpoint. The remaining offset is mainly due to friction phenomena.

Keywords: Centrifugal ring positioner, cascade control, control benchmark

Acknowledgements

First of all, I would like to thank Michel Kinnaert, supervisor of this master thesis, for the opportunity he has offered to me to conduct my master thesis in the Service d'Automatique et d'Analyse des Systèmes (SAAS department). His BA3 course about automation introduced me to the field of control systems and encouraged me to conduct my master thesis under his supervision. This enriching experience has allowed me to develop my knowledge and my skills in this attractive but challenging domain. I wish to thank him for his leadership, for his guidance and for his precious advices.

I also deeply thank Laurent Catoire, co-supervisor of this master thesis, for all the help he provided me during this project, for his availability and for the amount of time he devoted to this master thesis. A special thank for sharing his in-depth technical knowledge.

I would like to express my gratitude to Pierre Lambert for our discussion about system dynamics theory.

Finally, I would like to thank my parents and my sisters for the permanent support and encouragement they brought to me during these five years of studies, as well as for their experiences they shared with me. A deep thought for all my friends that have contributed to make my studies unforgettable, especially Romain, Joachim, Antoine and Simon.

Table of Contents

Abstract	I
Acknowledgements	II
Table of Contents	IV
List of Figures	VI
List of Tables	VII
Design of a didactic centrifugal ring positioner	1
1 State of the art	1
1.1 Introduction	1
1.2 Control systems pedagogical benchmarks	1
1.3 The inverted pendulum	2
1.3.1 Description of the system	2
1.3.2 Control of the inverted pendulum	2
1.3.3 System mathematical modelling	4
1.3.4 System variables measurements and sensors	6
1.4 The ball and beam	6
1.4.1 Description of the system	6
1.4.2 Control of the ball and beam	6
1.4.3 System mathematical modelling	7
1.4.4 System variables measurements and sensors	8
1.5 The centrifugal ring positioner	9
1.5.1 Description of the system	9
1.5.2 Control of the centrifugal ring positioner	9
1.5.3 System mathematical modelling	10
1.5.4 System variables measurements and sensors	10
1.6 Conclusion	11
2 Dynamic equations of the system	12
2.1 Parameters of the mathematical modelling	12
2.2 Mathematical development of the system dynamics	12
2.3 Linearisation	15
3 Design of the centrifugal ring positioner	18
3.1 Controller device	18
3.2 Actuator	19
3.2.1 Motor	19
3.2.2 Motor driver	20
3.3 Sensors	22
3.3.1 Position sensor	22
3.3.2 Angular velocity sensor	24
3.4 Design of the system	25
3.4.1 Motor support	25

3.4.2	Mobile ring and rod	25
3.4.3	Coupling pieces	27
3.4.4	Slip ring	28
3.5	Improvement of the position sensor signal	29
3.6	Wiring diagram	31
3.7	Final system	32
4	Control of the centrifugal ring positioner	34
4.1	Control strategy	34
4.2	Identification of the system transfer functions	35
4.2.1	Linearised system dynamics	35
4.2.2	Transfer function of the motor	36
4.2.3	Transfer function of the angular velocity-ring position subsystem	37
4.3	Inner loop: control of the motor angular velocity	38
4.4	Outer loop: control of the ring position	42
4.4.1	PID controller	42
4.4.2	PD controller	52
4.4.3	Comparison of outer loop controllers	55
5	Conclusion	57
Bibliography		62
Appendices		63
A Inertia tensor of the CRP		63
B Ring viscous friction coefficient		65
C Zero-Order Hold discretization method		67
D Simulink model of the CRP		70

List of Figures

1.1	Representation of the cart inverted pendulum (adapted from ^[1]). Parameters are defined in Table 1.1.	2
1.2	Control control strategy block diagram (inspired by ^[2]).	4
1.3	Representation of the inverted pendulum subsystems in cascade (adapted from ^[3]).	5
1.4	Representation of the first design (ball and beam balancer) of the ball and beam (inspired from ^[4]).	6
1.5	Representation of the second design of the ball and beam (adapted from ^[5]). Parameters are defined in Table 1.2.	6
1.6	Representation of the ball and beam subsystems in cascade.	8
1.7	Representation of the centrifugal ring positioner.	9
1.8	Representation of the system reported in ^[6]	9
1.9	Representation of the centrifugal ring positioner subsystems in cascade.	10
2.1	Simplified three-dimensional representation of the system.	13
2.2	Two-dimensional projection of the Figure 2.1.	13

3.1	Arduino DUE microcontroller ^[7]	19
3.2	Maxon RE25 Precious Metal Brushes CLL 10W gearmotor ^[8]	20
3.3	Escon 50/5 motor driver ^[9]	21
3.4	Output distance characteristics with the inverse of distance of the Sharp GP2Y0A41SK0F.	24
3.5	HEDS 5540 Encoder ^[10]	24
3.6	Three-dimensional model of the centrifugal ring positioner (realised on Solidworks).	25
3.7	Three-dimensional model of the motor support (designed on Solidworks).	27
3.8	Three-dimensional model of the ring (designed on Solidworks).	27
3.9	Three-dimensional model of the motor coupling piece (designed on Solidworks).	28
3.10	Three-dimensional model of the rod coupling piece (designed on Solidworks).	28
3.11	Illustration of the working principle of a slip ring (adapted from ^[11])	28
3.12	Noises in the position sensor signal due to the slip ring rotation (Arduino measurement corresponds to the sensor output voltage multiplied by 4096/3.3)	30
3.13	Wiring diagram of the centrifugal ring positioner	31
3.14	Top view picture of the centrifugal ring positioner	32
3.15	Profile view picture of the centrifugal ring positioner	33
4.1	Cascade control block diagram of the centrifugal ring positioner	35
4.2	Black-box motor model identification experiment	37
4.3	Root locus of the motor transfer function coupled to a P controller	39
4.4	Simulation of the motor angular velocity coupled to P controllers	40
4.5	Control of the motor angular velocity coupled to P controllers	41
4.6	Root locus of the system coupled to a PID controller ($T_d = 0.065$, $T_f = 0.008$ and $T_i = 0.150$)	43
4.7	Root locus of the system coupled to a PID controller ($T_d = 0.065$, $T_f = 0.008$ and $T_i = 0.150$) with $k_p = 0.15$	44
4.8	Bode diagram of the centrifugal ring positioner coupled to a PID ($k = 285$, $T_d = 0.065$, $T_f = 0.008$ and $T_i = 0.150$)	45
4.9	Comparison of centrifugal ring positioner step responses for ZOH and Tustin discretization methods	46
4.10	Comparison of centrifugal ring positioner Bode diagrams for ZOH and Tustin discretization methods	47
4.11	Control simulation of the centrifugal ring positioner coupled to a PID controller ($k = 285$, $T_d = 0.065$, $T_f = 0.008$ and $T_i = 0.150$)	48
4.12	Steering of the system from its rest position to the equilibrium point $(\bar{s}, \bar{\omega})$	49
4.13	Control of the centrifugal ring positioner coupled to a PID controller ($k = 285$, $T_d = 0.065$, $T_f = 0.008$ and $T_i = 0.150$)	50
4.14	Control of the centrifugal ring positioner coupled to a PID controller ($k = 216$, $T_d = 0.065$, $T_f = 0.013$ and $T_i = 0.160$)	51
4.15	Control of the centrifugal ring positioner coupled to a PD controller ($k = 328$, $T_d = 0.065$ and $T_f = 0.013$)	52

4.16	Control of the centrifugal ring positioner coupled to a PD controller ($k = 328$, $T_d = 0.065$ and $T_f = 0.013$).	53
4.17	Control simulation of the centrifugal ring positioner coupled to a PD controller ($k = 328$, $T_d = 0.065$ and $T_f = 0.013$).	54
4.18	Control of the centrifugal ring positioner coupled to a PD controller ($k = 328$, $T_d = 0.065$ and $T_f = 0.013$).	55
A.1	Simplified representation of the centrifugal ring positioner and decomposition in pieces for the inertia tensor calculation.	63
B.1	Experimental determination of the ring viscous friction coefficient. . .	65
C.1	Control of the centrifugal ring positioner coupled with a PID controller ($k = 285$, $T_d = 0.065$, $T_f = 0.008$ and $T_i = 0.150$) using ZOH discretization method.	67
C.2	Control of the centrifugal ring positioner coupled with a PID controller ($k = 216$, $T_d = 0.065$, $T_f = 0.013$ and $T_i = 0.160$) using ZOH discretization method.	68
C.3	Control of the centrifugal ring positioner coupled with a PD controller ($k = 328$, $T_d = 0.065$ and $T_f = 0.013$) using ZOH discretization method.	69
D.1	Simulink model of the cascade control of the centrifugal ring positioner.	70
D.2	Simulink model of the centrifugal ring positioner.	71

List of Tables

1.1	Parameters involved in the mathematical modelling of the cart inverted pendulum illustrated on Figure 1.1.	5
1.2	Parameters involved in the mathematical modelling of the ball and beam system illustrated on Figure 1.5.	7
1.3	Summary of the sensors usually used in the inverted pendulum and the ball and beam.	10
2.1	List of the parameters involved in the mathematical development of the centrifugal ring positioner dynamics.	12
3.1	Characteristics of the Maxon RE25 Precious Metal Brushes CLL 10W ^[12] .	20
3.2	Characteristics of the Escon 50/5 motor driver ^[9;12]	21
3.3	Comparative table between the IR Sharp GP2Y0A41SK0F and the US HC-SR04 ^[13;14]	23
3.4	Characteristics of the HEDS 5540 encoder ^[12]	24
3.5	Comparative table between the Senring H2056-0610 and the Moflon MT2042-S03 slip rings ^[11;15]	29
3.6	Standard deviations of the position sensor signal for different capacitor values.	31
4.1	Centrifugal ring positioner transfer functions.	35
4.2	Numerical values of position transfer function parameters.	37
4.3	Stability margins of the open inner loop.	40

4.4	Parameters of the PID controller for the centrifugal ring positioner . . .	44
4.5	Comparison of centrifugal ring positioner stability margins for ZOH and Tustin discretization methods.	47
4.6	Parameters of the new PID controller for the centrifugal ring positioner.	51
A.1	Pieces constituting the centrifugal ring positioner for the calculation of the tensor of inertia.	63

Chapter 1

State of the art

1.1 Introduction

This master thesis aims at designing, building and controlling a pedagogical benchmark for control system courses. This benchmark is called Centrifugal Ring Positioner (CRP). It consists of an unstable and non-linear system yet poorly reported in the literature. The aim of this centrifugal ring positioner is to become a laboratory device, allowing control engineering students to design controllers for stabilising the ring position.

This report first presents a state of the art aiming at presenting existing well-known control pedagogical benchmarks such as the inverted pendulum and the ball and beam. Then, the dynamic equations of the centrifugal ring positioner are derived based on mechanical theory concepts. Thereafter, the design of the system as well as the selection of its components such as actuator and sensors is discussed. Finally, the design of the controllers of the centrifugal ring positioner is detailed. Their performances are first tested in simulation and secondly on the real device.

1.2 Control systems pedagogical benchmarks

Control systems are present in many fields in today's world from manufacturing processes to consumer products. Implementation of new technological systems is partially possible thanks to the evolution of control theory, this evolution being closely linked to teaching activities and constantly evolving research. Practical experiments play an important role in control system theory understanding^[16]. Control engineering students and researchers should be able to make connections between theoretical and practical control systems concepts^[17]. It is essential for them to have the opportunity to face up practical cases to become aware of potential problems coming from real systems complexity. Practical experimentations allow to verify classical techniques, to perform model validation experiments, to develop new tools as well as to verify their implementation^[16;18]. Out of these reflections has flourished the idea of creating pedagogical benchmark systems. These control laboratory systems aim at performing experiments on real devices. Benchmarks should illustrate control theory aspects such as stabilisation of open-loop unstable systems, setpoint tracking and disturbance rejection^[19]. Requested characteristics for such benchmarks must be a good illustration of theoretical concepts, provide a good visual representation, easy use and understanding, and designed for low cost assembly^[20]. Among the best known control laboratory systems are the inverted pendulum and the ball and beam^[18].

Except one university project report^[6] written in Italian by a student from the Calabria University, Italy, no literature has been found about the system that aimed to be designed for this master thesis. Therefore, this literature review aims at highlighting similarities and differences existing between the centrifugal ring positioner and existing well-known benchmarks such as the inverted pendulum and the ball and beam. Specifically, cascade

control strategy and considered sensors referred to in the literature are relevant for the design of the centrifugal ring positioner.

1.3 The inverted pendulum

1.3.1 Description of the system

The inverted pendulum is a very well-known didactic system due to its high range of real-life applications such as self-balancing vehicles, robots and rockets launching^[21;22]. The interest in the use of the inverted pendulum for teaching and research activities has emerged due to the complexity of controlling this system. Even though its structure is relatively simple, the inverted pendulum presents a nonlinear, unstable and under-actuated behaviour making its control very challenging. Moreover, a lot of different designs of this system can be imagined (cart, 2 dimensional, rotational single-arm, rotational double-arm...) increasing thus the number of control challenges^[21;23]. In this literature review, we only focus on the cart inverted pendulum design that is constituted by a basic pendulum rooted on a cart able to move uniaxially. The design of this inverted pendulum is represented on Figure 1.1.

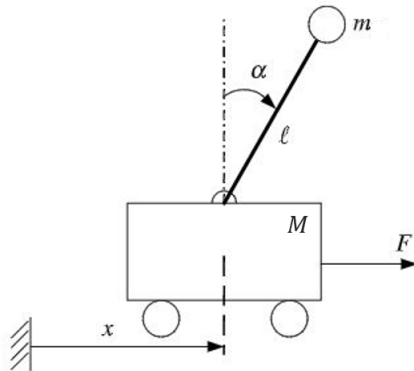


Figure 1.1 – Representation of the cart inverted pendulum (adapted from^[1]). Parameters are defined in Table 1.1.

The cart inverted pendulum has two equilibrium points, one stable and one unstable. The stable one consists of the downward pending position of the pendulum while the unstable one consists of the pendulum in its upward position^[16]. This second equilibrium point is obviously unstable since gravity makes constantly the pendulum coming back at its pending position as soon as the pendulum is not perfectly vertical.

1.3.2 Control of the inverted pendulum

The inverted pendulum is an attractive benchmark because it is constituted by three different control problems that can be divided into phases, namely the upswing phase, the stabilisation phase and the cart position control phase^[24]. The aim of the combination of the first two control phases is to stabilise the pendulum at its unstable equilibrium point, starting from the stable one. The upswing phase aims first at bringing the pendulum close to its upward position from its pending position. When the pendulum reaches a predefined zone close to the vertical, the purpose of the stabilisation phase is then to stabilise it around its unstable equilibrium position^[18;25]. The stabilisation problem can

be seen as the problem of trying to stabilise in the vertical position a stick lying on the palm of the hand^[22]. Some scientific studies treat this control problem in two steps, meaning implementing a controller for the upswing phase and another controller for the stabilisation of the pendulum at its upward position for small angle deviations. Other studies implement only one controller for the two phases^[26]. These two steps are achieved by acting on a motor making the cart move on the rail. This cart movement on the rail inspired the third phase, which aims to stabilise the pendulum at its upward equilibrium point at a given position coordinate of the cart. This third control problem constitutes an additional reason that makes the inverted pendulum so attractive. Indeed, considering only the upswing and the stabilisation phase, the cart inverted pendulum consists in a Single Input Single Output (SISO) system. Adding the control of the cart to the initial control problem extends the inverted pendulum to a Single Input Multiple Outputs (SIMO) system and creates an additional control challenge^[27].

Since the upswing phase or a similar one is not encountered for the control of the centrifugal ring positioner, only the stabilisation and the cart control phases of the inverted pendulum are considered in this literature review. Although it is rarely reported in the literature, both control problems can be treated using basic PID controllers. These controllers, based on linearised system dynamics, are sometimes criticised, specifically by Lee et al.^[1] and Irfan et al.^[21], for losing effectiveness if some uncertainties are present in the system model or if the system is submitted to important disturbances. Moreover, the double output control problem might render the use of conventional PID controller not fully adapted^[1;28]. However, PID have in some instances been successfully designed, at least in simulation. Wang indeed succeeded in simulating the stabilisation of the pendulum as well as the cart position control with conventional PID controllers, designing first the PID for the stabilisation phase regardless of the cart position. Then the PID for the cart position was designed and some modifications were done in the parameters of the stabilisation controller^[24]. Peker et al. have investigated cascade control of the cart inverted pendulum, stating that using two PID controller for controlling the pendulum angle and the cart position independently was not optimal and that the control strategy should be inspired by the inherent cascade structure of the system^[3].

Cascade is a control strategy that can be used to significantly improve the dynamics of a controlled system. This control strategy relies on an additional measured variable and on the implementation of an additional control loop. Cascade control implies dividing the system into two subsystems (an inner and an outer) and to implement a control loop for each of them (Figure 1.2). For a cascade control to be efficient, the inner loop dynamics must be faster than the outer loop dynamics. The interest of such a strategy is that it lowers the effect of disturbances in the inner loop before they affect the outer loop output. In other words, an additional control loop is implemented to regulate a variable potentially submitted to disturbances. Since this control loop has a faster dynamics than the main loop, it compensates the disturbances before they impact the manipulated variable. In a cascade structure, the setpoint of the inner loop is fixed by the outer loop controller output^[29;30;2].

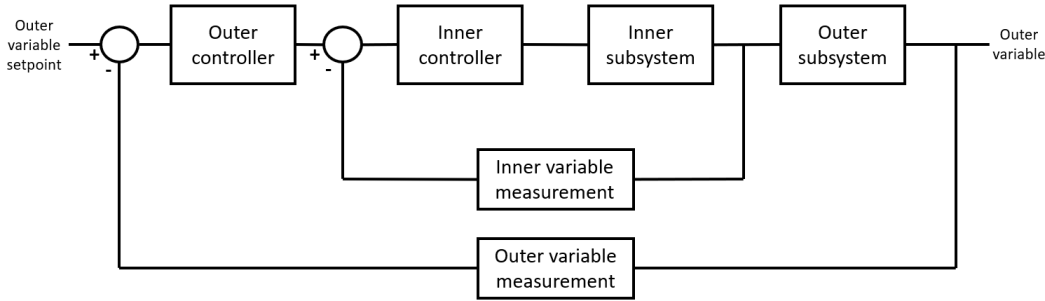


Figure 1.2 – Control control strategy block diagram (inspired by^[2]).

When considering a cascade control strategy for the cart inverted pendulum, the first subsystem consists of the pendulum rod while the second subsystem is the cart. By analogy to a basic control strategy in which the pendulum angle is first stabilised and then the cart position is controlled, the cascade strategy of the cart inverted pendulum relies on an inner loop consisting of stabilising the pendulum upward while the outer loop consists of controlling the cart position^[3;31]. Variations of the pendulum angle due to external disturbances that could affect the cart position are thus rapidly compensated in the inner loop. Cascade control of the inverted pendulum converts the initial SIMO inverted pendulum system into two SISO subsystems, allowing the use of conventional PID and showing better performances than the SIMO system^[31].

To supplement the discussion about the different control strategies applied on the inverted pendulum, let us note that there exists much more literature about modern non-linear control methods such as sliding mode or fuzzy logic control. These methods are reported to be more effective and more reliable and are therefore investigated to improve the performances of the inverted pendulum^[21;28]. The emergence of these modern control techniques is an additional reason that makes the inverted pendulum such an attractive experimental system resulting in large number of controllers implementation studies. These control methods are out of the scope of this master thesis.

1.3.3 System mathematical modelling

Regarding the dynamics of the inverted pendulum, the variables of interest are the position of the cart x and the vertical deviation angle of the pendulum α . In most of the mathematical models found in the literature, the input of the system consists of the force F applied via the motor to move the cart. Table 1.1 lists the parameters involved in the mathematical modelling of the cart inverted pendulum.

Parameters	
Angle of the pendulum	α
Position of the cart	x
Mass of the pendulum	m
Mass of the cart	M
Length of the pendulum	l
Cart friction coefficient	b
External force applied on the cart	F
Gravity acceleration	g
Inertia of the pendulum	I

Table 1.1 – Parameters involved in the mathematical modelling of the cart inverted pendulum illustrated on Figure 1.1.

Using these parameters, the dynamics of the inverted pendulum is modelled by equations 1.1 and 1.2^[21;22;3;31].

$$(M + m)\ddot{x} + mL\ddot{\alpha} \cos \alpha - ml\dot{\alpha}^2 \sin \alpha + b\dot{x} = F \quad (1.1)$$

$$(I + ml^2) \ddot{\alpha} - mgl \sin \alpha - ml\ddot{x} \cos \alpha = 0 \quad (1.2)$$

This system of equations is as expected non-linear, especially due to the terms $\dot{\alpha}^2$, $\sin \alpha$ and $\cos \alpha$. The cart friction coefficient is small compared to the other parameters and can be neglected^[3]. After performing linearisation around the equilibrium point $\alpha = 0$, transfer functions of each subsystem can be obtained. Equation 1.3 represents the general form of the transfer function of the inner subsystem, i.e. between the external force F and the pendulum angle α .

$$G_{in}(s) = \frac{\alpha(s)}{F(s)} = -\frac{a_i}{s^2 - b_i} \quad (1.3)$$

Equation 1.4 represents the general form of the transfer function of the outer subsystem, i.e. between the inner subsystem output α and the cart position x .

$$G_{out}(s) = \frac{X(s)}{\alpha(s)} = -\frac{(s^2 - a_o)}{b_o s^2} \quad (1.4)$$

where a_i , b_i , a_o and b_o are positive integers.

Figure 1.3 shows the cascade structure of the inverted pendulum. Controllers have to be designed for $G_{in}(s)$ and $G_{out}(s)$ and the control loops must be closed¹.

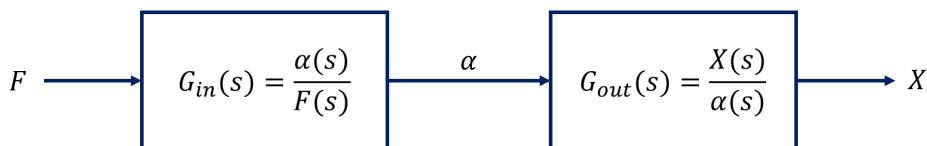


Figure 1.3 – Representation of the inverted pendulum subsystems in cascade (adapted from^[3]).

¹The inner loop can be unconsidered for the design of the outer loop controller. However, a very fast inner loop of unitary static gain is in this case required.

1.3.4 System variables measurements and sensors

With the aim of getting inspiration from existing didactic devices, it is also interesting to discuss briefly the instrumentation and more precisely the different sensors used in existing benchmarks, even if this aspect is usually poorly documented in the literature. Therefore, in order to extend the discussion about the inverted pendulum, a user manual of a cart inverted pendulum designed by *Quanser*² is also considered. Since the system has two outputs, it naturally needs two sensors. The main types of sensors used to measure these outputs are encoders and potentiometers. Rotary encoder can be coupled to the cart motor shaft and transform the angular motor position into a linear position for the cart^[1;32]. The cart position can also be measured with a potentiometer^[33]. Regarding the deviation angle of the pendulum rod, this can be measured either with a rotary encoder^[1;32;17] or with a potentiometer^[33].

1.4 The ball and beam

1.4.1 Description of the system

The ball and beam is another very famous non-linear and unstable benchmark. Like the inverted pendulum, the ball and beam is widely used to implement and analyse modern control algorithms due to its simplicity of construction^[34;35]. As its name implies, this system is composed by a ball lying on a beam. A motor is connected to the beam in order to make it rotate. Many different ball and beam systems can be constructed but two main designs are referred to in the literature. In the first design (Figure 1.4), also called ball and beam balancer, the motor is connected to the middle of the beam, making the beam able to rotate around its central axis^[34]. In the second design (Figure 1.5), one end of the beam is rooted and is only able to rotate, creating an angle with the horizontal while the other end is able to move vertically thanks to a level arm connected to a motor. In both cases, the tilt angle α of the beam according to the horizontal can be changed by playing on the position angle of the motor θ and the ball can roll freely along the beam^[29;36;37]. From now, only the second design is considered.

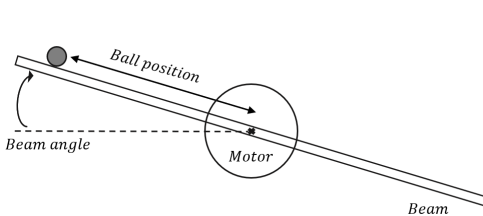


Figure 1.4 – Representation of the first design (ball and beam balancer) of the ball and beam (inspired from^[4]).

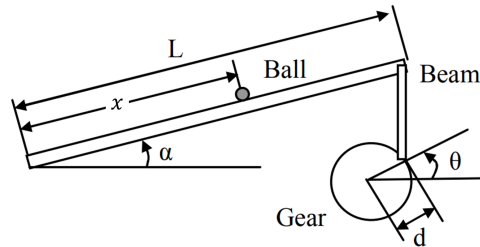


Figure 1.5 – Representation of the second design of the ball and beam (adapted from^[5]). Parameters are defined in Table 1.2.

1.4.2 Control of the ball and beam

Compared to the inverted pendulum which has a control problematic that can be divided into three phases, the ball and beam only has one control problem. That consists in

²*Quanser* is a company specialised in the design and manufacture of teaching and research platforms in multiple fields such as control systems and robotics (<https://www.quanser.com/about/>).

controlling the position of the ball on the beam and in rejecting potential disturbances. This is achieved by changing the tilt angle of the beam via the motor^[37;38]. This problem therefore consist of a SISO problem, with the ball position as output and the motor voltage as input. Implementation of linear controllers such as basic PD or PID as well as non-linear controller such as fuzzy or fractional order is found in literature. However, according to Taifour et al.^[38], considering one overall system with motor voltage as input and ball position as output is too complex and obtaining proper control results is quite complex. This is probably the reason why, no matter the kind of controller, a recurrent control strategy is found in the literature: the cascade control. The advantages of cascade control have already been discussed in Section 1.3.2. The control scheme is similar to the inverted pendulum, consisting of two subsystems in series. The principle is now however different. For the inverted pendulum, the cascade control strategy aims to overcome the SIMO problem, i.e. controlling the pendulum angle and the cart position. The idea is to take advantage of the faster behaviour of the stabilisation loop to improve the performances of the cart control loop. Since the ball and beam is initially a SISO system, the cascade control is applied differently. Indeed, the ball and beam can be seen as a combination of two subsystems, the first one consisting of the ball and the beam and the second one consisting of the motor. Cascade control means thus considering the motor angular position as an intermediate output directly linked to the main system input (the motor voltage). This requires the implementation of an inner loop aiming to control the motor angle position with respect to a reference angle and the implementation of an outer loop aiming to control the ball position^[38;29]. This configuration allows not to rely directly on the motor voltage to control the ball position. Cascade control aims thus in this problem to mitigate frictional effects on the actuator as well as to speed up its dynamics to improve the overall system dynamics.

1.4.3 System mathematical modelling

Table 1.2 contains the parameters of the mathematical modelling of the ball and beam.

Parameters	
Position of the ball on the beam	x
Angle of the beam	α
Angular position of the motor	θ
Mass of the ball	m
Inertia of the ball	I
Radius of the ball	R
Gravity acceleration	g
Lever arm offset	d
Length of the beam	L

Table 1.2 – Parameters involved in the mathematical modelling of the ball and beam system illustrated on Figure 1.5.

Equation 1.5 represents the Newton's second law of motion applied to the ball. This equation gives the relation between the position of the ball on the beam as a function of the angle of the beam^[29;30;5]. This equation is non-linear due to the term $\sin \alpha$.

$$\left(m + \frac{I}{R^2} \right) \ddot{x} + mg \sin \alpha = 0 \quad (1.5)$$

For small angles variations, the link between the beam angle and the motor angular position can be considered as linear^[30;37].

$$\alpha = \frac{d}{L}\theta \quad (1.6)$$

Linearising equation 1.5 around an equilibrium point and coupling it with equation 1.6 gives the transfer function between the position of the ball and the motor angular position, i.e. the outer subsystem transfer function (general form of the transfer function given by the equation 1.7).

$$G_{out}(s) = \frac{X(s)}{\theta(s)} = -\frac{a_o}{s^2} \quad (1.7)$$

The inner subsystem transfer function is simply given by the DC motor transfer function (general form of the transfer function given by the equation 1.8)^[30].

$$G_{in}(s) = \frac{\theta(s)}{V(s)} = \frac{a_i}{s(b_is + 1)} \quad (1.8)$$

where a_o , a_i and b_i are positive integers³.

Figure 1.6 illustrates the cascade structure of the two subsystems of the ball and beam.

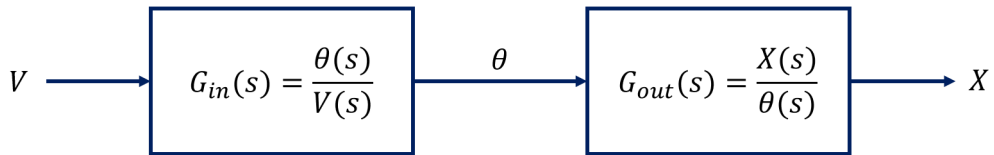


Figure 1.6 – Representation of the ball and beam subsystems in cascade.

1.4.4 System variables measurements and sensors

Like the inverted pendulum, let us consider the different sensors usually used in the ball and beam. Such a system is a SISO system and a single sensor, used to measure the ball position, could therefore be sufficient. The most common instrument to measure the ball position is a potentiometer, taking advantage on the contact of the ball with the beam^[30;36;34]. This is also the sensor reported in the user manual of the ball and beam designed by *Quanser*. Other position sensors such as an ultrasonic sensor can be used^[38]. Nevertheless, as previously indicated, the poor performances sometimes obtained by a single variable measurement lead to the implementation of cascade control. This implies the introduction of a new measurement, which is the motor angular position in case of the ball and beam. Without this additional sensor, it would not be possible to implement a cascade control. The motor angular position is usually measured by a rotary potentiometer^[34] or by an encoder^[30;39].

³The values of these parameters differ from the ones defined in Section 1.3.3.

1.5 The centrifugal ring positioner

1.5.1 Description of the system

The centrifugal ring positioner, represented on Figure 1.7, has been inspired by the system reported in the university project report^[6] represented on Figure 1.8. Like the inverted pendulum and the ball and beam, it is a non-linear unstable system. It is composed by a mobile hollow cylinder able to slide on a tilted rod. This rod is coupled to the shaft of a motor and can therefore rotate around the vertical axis. When the centrifugal force exerted on the mobile due to the rotation overcomes the gravity, the cylinder slides towards the end of the rod. This system is unstable since the rotational velocity needed to move the mobile from its rest position makes the cylinder sliding further and further from its initial position. Equilibrium points are reached by lowering this velocity until position on the rod where the centrifugal force is balanced by the gravity.

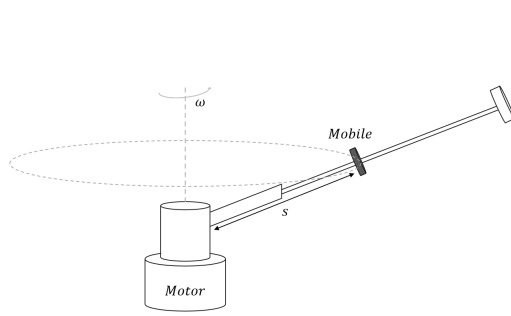


Figure 1.7 – Representation of the centrifugal ring positioner.

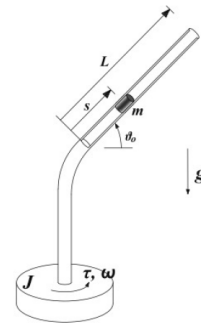


Figure 1.8 – Representation of the system reported in^[6].

1.5.2 Control of the centrifugal ring positioner

The aim of the control strategy applied to the centrifugal ring positioner is to control the position of the cylinder according to a setpoint by acting on the rotational velocity via the current fed to the motor. The centrifugal ring positioner is thus a SISO system. As it will be further developed, a transfer function between the position of the mobile and the current of the motor can be derived. However, like the ball and beam, the centrifugal ring positioner could present significant disturbances such as friction at the level of the actuator and designing one single controller for this system is probably not the most efficient control strategy. Moreover, similarities in working principle can be found with the ball and beam, more than with the inverted pendulum. Indeed, for both systems, the aim is to use indirectly the angular position or velocity of a motor to control the position of a mobile (a ball or a ring). By analogy, we can look at the centrifugal ring positioner as a combination of two subsystems and consider a cascade control strategy. Like the ball and beam, the inner subsystem consists of the motor and the outer subsystem consists in the mobile and the tilted rod instead of the ball and the beam. For this reason and for all the advantages brought by this strategy, it would therefore be interesting to consider a cascade control for this system, for the same reason it is reported in the literature for the ball and beam, thus by taking advantage of an additional measurement to make the actuator dynamics faster.

1.5.3 System mathematical modelling

The complete development of the mathematical modelling of the centrifugal ring positioner is performed in Section 2. Based on this modelling, transfer functions for the centrifugal ring positioner subsystems can be derived. The inner subsystem transfer function, represented by $G_{in}(s)$, consists of the motor where input is the motor current i and output is the angular velocity ω . The outer subsystem, represented by $G_{out}(s)$, has the motor angular velocity as input and the mobile position s as output. The cascade structure of these subsystems is represented on Figure 1.9. More about these transfer functions and the cascade control strategy is developed in Section 4.

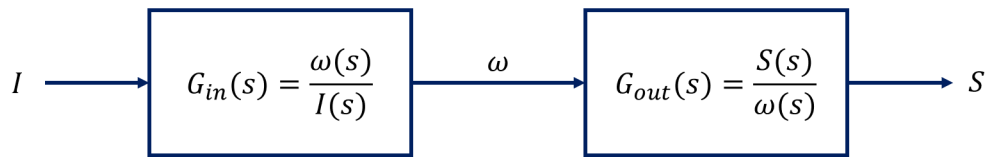


Figure 1.9 – Representation of the centrifugal ring positioner subsystems in cascade.

1.5.4 System variables measurements and sensors

It is also interesting to make a comparison between the inverted pendulum, the ball and beam and the centrifugal ring positioner in term of measurement problematic. As a reminder, Table 1.3 lists the sensors used in the inverted pendulum and in the ball and beam.

	Measurement	Sensors
Inverted Pendulum	Pendulum angle	Rotary potentiometer Encoder
	Cart position	Rotary potentiometer Encoder
Ball and beam	Motor angular position	Rotary potentiometer Encoder
	Ball position	Potentiometer Ultrasonic sensor

Table 1.3 – Summary of the sensors usually used in the inverted pendulum and the ball and beam.

Regarding the mobile position, the centrifugal ring positioner measurement problematic has most similarities with the ball position measurement in the ball and beam. Potentiometer and ultrasonic sensors may therefore be an appropriate sensor choice for the mobile measurement. As discussed previously, considering a cascade control for the centrifugal ring positioner implies the need of a motor angular velocity sensor. This velocity can be derived from the change in motor angular position. Therefore, motor angular position sensor such as rotary potentiometer and encoder used in the inverted pendulum and in the ball and beam may be interesting sensors. The selection of sensors for the centrifugal ring positioner is developed in Section 3.3.



1.6 Conclusion

Taking into account the lack of literature about the centrifugal ring positioner, two of the most famous didactic systems for control theory, namely the inverted pendulum and the ball and beam, have been introduced. All three systems present similar attractive characteristics such as instability and non-linearity. The different control characteristics and challenges of each system have been discussed. These three systems may illustrate a enhanced control strategy, specifically the cascade control. This literature review indicated that even if cascade control is implemented for the same benefits for the inverted pendulum and for the ball and beam, their implementation and working principles are different. As such, it does seem that the centrifugal ring positioner presents more similarities with the ball and beam than with the inverted pendulum. The detailed control of the centrifugal ring positioner is developed in Section 4. The different measurement problems of each system have also been tackled aiming to open up lines thought about sensors to use for the centrifugal ring positioner. A deeper discussion about the sensors selection for the centrifugal ring positioner is performed in Section 3.3.

Chapter 2

Dynamic equations of the system

2.1 Parameters of the mathematical modelling

Table 2.1 contains the different parameters that are involved in the mathematical development of the centrifugal ring positioner dynamics. The following table will serve as the reference for all the parameters mentioned further within this chapter.

Parameters					
Mass of the mobile	m	kg	Angular velocity of the CRP	ω	rad/s
Tilt angle of the rod	θ	deg	Distance between the mobile and the rotational axis	r	m
Position of the mobile on the rod	s	m	Mobile viscous friction coefficient	c	kg/s
Weight of the mobile	G	N	Normal reaction of the rod on the mobile	N	N
Viscous friction force against mobile movement	F_f	N	Relative velocity of the mobile	v_{rel}	m/s
Relative acceleration of the mobile	a_{rel}	m/s^2	Centripetal acceleration of the mobile	a_c	m/s^2
Coriolis acceleration of the mobile	a_{Cor}	m/s^2	Acceleration of gravity	g	m/s^2
Velocity of the centre of mass of the CRP	v_G	m/s	Velocity of the point O	v_O	m/s
Angular momentum of the CRP	M_O	$kg\ m^2/s$	External momentum applied in O	$m_{e,O}$	Nm
Inertia tensor of the CRP	J	$kg\ m^2$	Motor momentum applied in O	$m_{mot,O}$	Nm
Motor current	i	A	Motor torque constant	K	N/A
Motor viscous friction coefficient	f	$Nm\ s$	Motor resistive torque	C_r	Nm

Table 2.1 – List of the parameters involved in the mathematical development of the centrifugal ring positioner dynamics.

2.2 Mathematical development of the system dynamics

In order to derive an equation that links the position of the mobile on the rod and the angular velocity of the system, let us write the second Newton's law of motion^[40]. Figure

2.1 illustrates the mobile on the rod, represented by a sphere, rotating around the vertical axis, namely the axis z in the fixed system of axes xyz . To obtain the motion equation of the mobile, it is appropriate to introduce two new axes systems: the XYZ system rotating around the vertical z axis and the tYn system centred in the mobile position. Figure 2.2 represents a two-dimensional projection of Figure 2.1 and also indicates the different forces acting on the mobile.

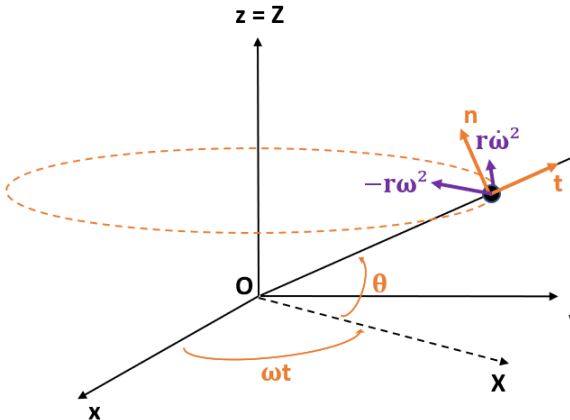


Figure 2.1 – Simplified three-dimensional representation of the system.

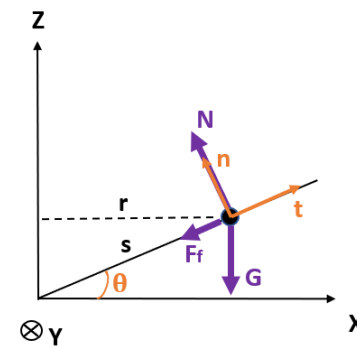


Figure 2.2 – Two-dimensional projection of the Figure 2.1.

In a rotating axes system, the motion law is expressed by equation 2.1^[40].

$$\sum \vec{F} = m\vec{a}_{rel} + m\vec{a}_c + m\vec{a}_{Cor} \quad (2.1)$$

Since we are interested in the motion of the mobile on the rod, it is more convenient to work in the tYn system of axes. Let us tackle individually each term of the motion equation.

The relative acceleration of the mobile is simply given by the second derivative of its position.

$$\vec{a}_{rel} = \ddot{s}\vec{1}_t \quad (2.2)$$

The centripetal acceleration is given by the following equation.

$$\begin{aligned} \vec{a}_c &= -r\omega^2\vec{1}_X + r\dot{\omega}\vec{1}_Y = -s\omega^2\cos\theta\vec{1}_X + s\dot{\omega}\cos\theta\vec{1}_Y \\ &= -s\omega^2\cos\theta(\cos\theta\vec{1}_t - \sin\theta)\vec{1}_n + s\dot{\omega}\cos\theta\vec{1}_Y \end{aligned} \quad (2.3)$$

The Coriolis acceleration is given by the equation here below.

$$\vec{a}_{Cor} = 2\vec{\omega} \times \vec{v}_{rel} = 2\omega\vec{1}_Z \times \dot{s}\vec{1}_t = \beta\vec{1}_Y \quad (2.4)$$

where β is a quantity containing the result of the vector product.

As it will be further detailed, only terms oriented towards $\vec{1}_t$ are relevant for the motion equation of the mobile. The result of this vector product is oriented towards $\vec{1}_Y$ and must therefore not be calculated. As represented on Figure 2.2, there are three forces acting on

the mobile. Those are the gravity, the normal reaction of the rod on the mobile and the viscous friction against the mobile movement.

$$\vec{G} = -mg\vec{1}_Z = -mgsin\theta\vec{1}_t - mgcos\theta\vec{1}_n \quad (2.5)$$

$$\vec{N} = N\vec{1}_n \quad (2.6)$$

$$\vec{F}_f = -c\dot{s}\vec{1}_t \quad (2.7)$$

By substituting all of these expressions in equation 2.1, the motion equation of the mobile is obtained.

$$\begin{aligned} m\ddot{s}\vec{1}_t &= -mgsin\theta\vec{1}_t - mgcos\theta\vec{1}_n + N\vec{1}_n - c\dot{s}\vec{1}_t + ms\omega^2cos\theta(cos\theta\vec{1}_t - sin\theta\vec{1}_n) \\ &\quad - ms\dot{\omega}cos\theta\vec{1}_Y - m\beta\vec{1}_Y \end{aligned} \quad (2.8)$$

Since only the translation along the rod axis, namely $\vec{1}_t$, is relevant, this equation simplifies as follows.

$$m\ddot{s} = -mgsin\theta - c\dot{s} + ms\omega^2cos^2\theta \quad (2.9)$$

This equation thus links the acceleration of the mobile on the rod to the rotational velocity of the system.

The next step of the dynamic modelling consists in including the input of the system, i.e. the motor current. To achieve that, let us apply the angular momentum theorem in O . The point O is defined as the intersection of the rod with the vertical motor shaft (see Figure 2.1), its velocity is therefore zero and the angular momentum theorem equation is simplified (equation 2.10)^[40].

$$\frac{d\vec{M}_O}{dt} = m\vec{v}_G \times \vec{v}_O + \vec{m}_{e,O} = \vec{m}_{e,O} \quad (2.10)$$

The angular momentum is given by the following matrix product.

$$\begin{aligned} \vec{M}_O &= \bar{\vec{J}} \cdot \vec{\omega} = \begin{pmatrix} j_{11} & j_{12} & j_{13} \\ j_{21} & j_{32} & j_{23} \\ j_{31} & j_{32} & j_{33} \end{pmatrix} \begin{pmatrix} 0 \\ 0 \\ \omega \end{pmatrix} \\ &= j_{13}\omega\vec{1}_X + j_{23}\omega\vec{1}_Y + j_{33}\omega\vec{1}_Z \\ &= M_X\vec{1}_X + M_Y\vec{1}_Y + M_Z\vec{1}_Z \end{aligned} \quad (2.11)$$

The derivative of the angular momentum accounting for the fact that the axes XYZ are rotating is given by the equation 2.12.

$$\begin{aligned} \frac{d\vec{M}_O}{dt} &= \left(\frac{dM_X}{dt}\vec{1}_X + \frac{dM_Y}{dt}\vec{1}_Y + \frac{dM_Z}{dt}\vec{1}_Z \right) + \vec{\omega} \times \vec{M}_O \\ &= \left(\frac{dM_X}{dt} - \omega M_Y \right) \vec{1}_X + \left(\frac{dM_Y}{dt} + \omega M_X \right) \vec{1}_Y + \frac{dM_Z}{dt}\vec{1}_Z \end{aligned} \quad (2.12)$$

However, let us remember that we are looking for a relation involving the motor current. According to the mechanical equation of the motor¹, the external momentum acting on

¹The resistive torque of the motor C_r is assumed to be constant.

the point O due to the motor is given by the equation 2.13.

$$\begin{aligned}\vec{m}_{mot,O} &= \vec{C} - \vec{C}_r - \vec{C}_f \\ &= K.i \vec{1}_Z - C_r \vec{1}_Z - f.\omega \vec{1}_Z\end{aligned}\quad (2.13)$$

Since these momentum's are only oriented towards $\vec{1}_Z$ and that there is no additional Z -oriented momentum acting on O , the angular momentum theorem equation is simplified using equations 2.12 and 2.13.

$$\frac{dM_Z}{dt} = K.i - C_r - f.\omega \quad (2.14)$$

As we can see from this equation, the angular momentum theorem only involves one term of the angular momentum and therefore only the element j_{33} of the inertia tensor of the system. The detailed calculation of this element is performed in Appendix A. This element is composed of a constant term i_{33} and a non-constant term varying with the position of the mobile on the rod. The derivative of M_Z is thus given by equation 2.15.

$$\begin{aligned}\frac{dM_Z}{dt} &= \frac{d}{dt} ((i_{33} + ms^2 \cos^2 \theta) \omega) \\ &= (i_{33} + ms^2 \cos^2 \theta) \dot{\omega} + 2ms\dot{s}\omega \cos^2 \theta\end{aligned}\quad (2.15)$$

Finally, substituting this expression in equation 2.14 leads to the equation linking the motor current with the angular velocity of the system and the mobile position (equation 2.16).

$$K.i - C_r - f.\omega = i_{33}\dot{\omega} + ms^2 \cos^2 \theta \dot{\omega} + 2ms\dot{s}\omega \cos^2 \theta \quad (2.16)$$

Coupling the equations 2.9 and 2.16 and performing some mathematical manipulations leads to the system 2.17, modelling the dynamics of the centrifugal ring positioner.

$$\begin{cases} \ddot{s} = -g \sin \theta - \frac{c}{m} \dot{s} + s \omega^2 \cos^2 \theta = f_s(s, \dot{s}, \omega) \\ \dot{\omega} = \frac{1}{(i_{33} + ms^2 \cos^2 \theta)} (Ki - C_r - f\omega - 2ms\dot{s}\omega \cos^2 \theta) = f_\omega(s, \dot{s}, \omega, i) \end{cases} \quad (2.17)$$

2.3 Linearisation

The newly obtained system of equations 2.17 is non-linear. In order to be able to obtain a transfer function for the centrifugal ring positioner, this system of equations must be linearised around an equilibrium point. A classical equilibrium point is obtained by cancelling the derivative of s and ω , leading to $\dot{s} = 0$, $\ddot{s} = 0$ and $\dot{\omega} = 0$.

$$\begin{cases} 0 = -g \sin \theta + s \omega^2 \cos^2 \theta \\ 0 = \frac{1}{(i_{33} + ms^2 \cos^2 \theta)} (Ki - C_r - f\omega) \end{cases} \quad (2.18)$$

Hence, the equilibrium point is given by:

$$\begin{cases} \bar{s} = \frac{g \sin(\theta)}{\bar{\omega}^2 \cos^2(\theta_0)} \\ \bar{\omega} = \frac{K\bar{i} - C_r}{f} \end{cases}$$

Small deviations according to the equilibrium point need to be considered to perform the linearisation. These deviations variables are given by:

$$\begin{cases} s \simeq \delta s \\ \dot{s} \simeq \delta \dot{s} \\ \ddot{s} \simeq \delta \ddot{s} \\ \omega \simeq \delta \omega \\ i \simeq \delta i \end{cases}$$

Using these deviations variables, the linearised system is given by system 2.21.

$$\begin{cases} \delta \ddot{s} = \frac{\partial f_s}{\partial s} \Big|_{\bar{x}, \bar{i}} \delta s + \frac{\partial f_s}{\partial \dot{s}} \Big|_{\bar{x}, \bar{i}} \delta \dot{s} + \frac{\partial f_s}{\partial \omega} \Big|_{\bar{x}, \bar{i}} \delta \omega \\ \delta \omega = \frac{\partial f_\omega}{\partial s} \Big|_{\bar{x}, \bar{i}} \delta s + \frac{\partial f_\omega}{\partial \dot{s}} \Big|_{\bar{x}, \bar{i}} \delta \dot{s} + \frac{\partial f_\omega}{\partial \omega} \Big|_{\bar{x}, \bar{i}} \delta \omega + \frac{\partial f_\omega}{\partial i} \Big|_{\bar{x}, \bar{i}} \delta i \end{cases} \quad (2.21)$$

where \bar{x} is the equilibrium state vector (defined below in equation 2.23).

Replacing the functions f_s and f_ω by their expressions, calculating their derivatives in the equilibrium point and considering that $\bar{s} = 0$ by definition leads to the linearised system of equations 2.22.

$$\begin{cases} \delta \ddot{s} = \bar{\omega}^2 \cos^2 \theta \delta s - \frac{c}{m} \delta \dot{s} + 2\bar{s}\bar{\omega} \cos^2 \theta \delta \omega \\ \delta \dot{\omega} = -\frac{2m\bar{s}\bar{\omega} \cos^2 \theta}{(i_{33} + m\bar{s}^2 \cos^2 \theta)} \delta \dot{s} - \frac{f}{(i_{33} + m\bar{s}^2 \cos^2 \theta)} \delta \bar{\omega} + \frac{K}{(i_{33} + m\bar{s}^2 \cos^2 \theta)} \delta i \end{cases} \quad (2.22)$$

The initial system is now linearised around an equilibrium point. In order to obtain a state-space representation, we have to define the state vector x , the equilibrium vector \bar{x} as well as the input u of the system.

$$x = \begin{cases} x_1 = \delta s \\ x_2 = \delta \dot{s} \\ x_3 = \delta \omega \end{cases} \quad \bar{x} = \begin{cases} \bar{x}_1 = \bar{s} \\ \bar{x}_2 = \bar{\dot{s}} \\ \bar{x}_3 = \bar{\omega} \end{cases} \quad u = \delta i \quad (2.23)$$

By substituting this state vector, this equilibrium vector and this input in the system 2.22, we obtain the following state-space representation.

$$\begin{cases} \dot{x}_1 = x_2 \\ \dot{x}_2 = \bar{x}_3^2 \cos^2 \theta x_1 - \frac{c}{m} x_2 + 2\bar{x}_1 \bar{x}_3 \cos^2 \theta x_3 \\ \dot{x}_3 = -\frac{2m\bar{x}_1 \bar{x}_3 \cos^2 \theta}{(i_{33} + m\bar{x}_1^2 \cos^2 \theta)} x_2 - \frac{f}{(i_{33} + m\bar{x}_1^2 \cos^2 \theta)} x_3 + \frac{K}{(i_{33} + m\bar{x}_1^2 \cos^2 \theta)} u \end{cases} \quad (2.24)$$

This state-space representation can be rewritten in matrix form.

$$\begin{bmatrix} \dot{x}_1 \\ \dot{x}_2 \\ \dot{x}_3 \end{bmatrix} = \begin{bmatrix} 0 & 1 & 0 \\ \bar{x}_3^2 \cos^2 \theta & -\frac{c}{m} & 2\bar{x}_1 \bar{x}_3 \cos^2 \theta \\ 0 & -\frac{2m\bar{x}_1 \bar{x}_3 \cos^2 \theta}{i_{33} + m\bar{x}_1^2 \cos^2 \theta} & -\frac{f}{i_{33} + m\bar{x}_1^2 \cos^2 \theta} \end{bmatrix} \begin{bmatrix} x_1 \\ x_2 \\ x_3 \end{bmatrix} + \begin{bmatrix} 0 \\ 0 \\ \frac{K}{i_{33} + m\bar{x}_1^2 \cos^2 \theta} \end{bmatrix} u \quad (2.25)$$

The output variables of the state-space representation must be defined. Since we aim to control the position of the mobile as well as the rotational velocity of the system, it makes sense to chose x_1 and x_3 as output.

$$y = \begin{bmatrix} \delta s \\ \delta \omega \end{bmatrix} = \begin{bmatrix} x_1 \\ x_3 \end{bmatrix}$$

Again, the output equations of the system can be expressed in matrix form.

$$\begin{bmatrix} y_1 \\ y_2 \end{bmatrix} = \begin{bmatrix} 1 & 0 & 0 \\ 0 & 0 & 1 \end{bmatrix} \begin{bmatrix} x_1 \\ x_2 \\ x_3 \end{bmatrix} + \begin{bmatrix} 0 \\ 0 \end{bmatrix} u \quad (2.26)$$

Chapter 3

Design of the centrifugal ring positioner

This section aims at describing the design of the centrifugal ring positioner and at considering the selection of the different components that are required to implement such a system. Firstly, the choice of the controller device and the selection of the appropriate actuator is discussed. Thereafter, the selection of the different sensors is addressed. Then, the structure of the centrifugal ring positioner and the design of the pieces is discussed. Finally, the general wiring diagram of the system is presented as well as some pictures of the real device.

3.1 Controller device

The controller device acts like the brain of the centrifugal ring positioner. It encompasses all the programming part, from sensor measurements acquisition to control algorithms. Two possibilities were envisaged regarding the controller device, either using a National Instruments (NI) PCI-6014 acquisition board directly integrated to the SAAS computers or using an Arduino microcontroller. Regarding the Arduino, a selection had to be done among the different models that exist. It has been decided to consider an Arduino DUE for the controller device because it presents, by opposition to other most usual Arduino models, a true Digital to Analog Converter (DAC) output that can be very appropriate to command the motor via the motor driver. Moreover, this model was available on stock in the SAAS department.

Since the centrifugal ring positioner aims to become an laboratory device, the NI PCI-6014 was an interesting solution, allowing to work directly on Matlab via the SAAS computers. As it will be more detailed in Section 3.2.2, most of the considered motor drivers are driven by the controller through an analog input voltage from -10 V to 10 V. The NI PCI-6014 is able to directly provide a command signal between -10 V and 10 V while the DAC output of the Arduino DUE can only provide signals from 0.55 V to 2.75 V. Using an Arduino DUE could therefore imply thereafter the potential need of some transition electronics to convert this signal into the proper voltage range. However, the portability offered by the Arduino that is not offered by the NI PCI-6014 connected to the SAAS computers would allow to make the system transportable which could be appropriate in some cases for demonstrations for example. This portability side would also offer the possibility of working on the thesis from home. In addition, the Arduino offers the opportunity to work at higher computational frequency than the NI PCI-6014. These last two features of the Arduino have oriented the choice of the controller device towards the Arduino DUE.



Figure 3.1 – Arduino DUE microcontroller^[7].

3.2 Actuator

The actuator is the device that allows the controller to act on the system. Based on real-time measurements and on control algorithms, the microcontroller calculates the required command for the actuator. The main requirements for the actuator of the centrifugal ring positioner is to be able to provide the needed torque and to rotate at the needed velocities in extreme cases¹. The actuator consists of a motor fed in current by a motor driver.

3.2.1 Motor

Due to potential shipping delays in case of the motor had to be bought from a manufacturer, the motor had to be selected at the beginning of the thesis. For this reason, exact values of the required angular velocities and torques were not available when the selection of the motor had to be conducted. Those had to be estimated from control simulations themselves based on estimated system parameters and design as well as based on preliminary controllers. It resulted from these simulations that in extreme cases, the system must rotate at about 130 rpm and the motor should be able to provide a torque of approximately 1.5 Nm. Regarding the torque, a security factor of 100% was taken into account for unquantified parameters such as friction. Motors from the manufacturer Maxon have been investigated. In most of the cases, the nominal torques that can be provided by these motors are of the order of hundreds mNm which was clearly insufficient for our application. One way to increase the torque of a motor is to couple it to a reduction gear, leading to a device called gearmotor. The gearmotor also converts the velocity of the motor into a lower velocity with a certain reduction factor.

To avoid shipping delays and unnecessary costs, a motor used previously for other applications in the SAAS department has been first investigated. This motor is the Maxon RE25 Precious Metal Brushes CLL 10W (Figure 3.2). This motor was already coupled to a reduction gear and to an encoder. Table 3.1 contains the relevant characteristics of this gearmotor.

¹Extreme cases are reached for very short times when the mobile is submitted to a important setpoint change.



Figure 3.2 – Maxon RE25 Precious Metal Brushes CLL 10W gearmotor^[8].

Maxon RE25 Precious Metal Brushes CLL 10W		
Nominal voltage	V_{nom}	24 V
Nominal velocity	ω_{nom}	4130 rpm
Maximal velocity	ω_{max}	5500 rpm
Nominal current	I_{nom}	0.652 A
Torque constant	K	43.9 mNm/A
Reduction	η_g	35:1

Table 3.1 – Characteristics of the Maxon RE25 Precious Metal Brushes CLL 10W^[12].

This motor has been chosen since it fulfils the requirements. Regarding the velocity, accounting for the reduction gear, the nominal velocity of the gearmotor is 118 rpm (ω_{nom}/η_g) which is lower than the 130 rpm required in extreme cases. Nevertheless, such high velocity is only required for very short times meaning that the motor can exceed its nominal velocity. It was however necessary to check that this velocity does not exceed the maximal velocity of the gearmotor (about 157 rpm (ω_{max}/η_g)), which is indeed not the case.

For very short times, it can be assumed that a current four times larger than the nominal current can be supplied to the motor. This means that when needed, the following torque can be provided by the motor:

$$\tau = 4 \times I_{nom} \times K \times \eta_g = 4.007 \text{ Nm}$$

This torque is actually more than 100% higher than the 1.5 Nm required for the system. The motor Maxon RE25 Precious Metal Brushes CLL 10W coupled to a gear reduction of 35 was therefore an appropriate gearmotor for the centrifugal ring positioner.

3.2.2 Motor driver

To control a motor with a microcontroller, a motor driver is required. Let us remind ourselves that the selected microcontroller is an Arduino DUE. Basically, the motor driver receives an analog command signal from the Arduino and converts it into a specific current to feed the motor.

Due to their frequent uses in the SAAS department, it has been decided to use an Escon motor driver. These drivers contain their own internal current control loop. That means that we can assume that the Escon exactly provides to the motor the current requested by the Arduino². These motor drivers also present an interesting feature consisting of an internal motor velocity control loop. An encoder can directly be connected to the Escon and the driver can then automatically control the motor velocity by adjusting the feeding current. This feature would probably not be used for our application since it would remove the didactic control aspect of the system. However, having the possibility of relying on this internal velocity control was potentially interesting for preliminary mobile position control tests, allowing in this way to only focus on the mobile position and not on the velocity

²This assumption is correct while saturation is not reached.

control. Thanks to their availability in the SAAS department, it has been decided to used the Escon 50/5 model (Figure 3.3). Some relevant characteristics of this motor driver are listed in Table 3.2.

ESCON 50/5 Motor Driver		
Operating voltage	V_{nom}	10 V to 50 V
Output current	$I_{con}/I_{max} (<20s)$	5 A/15 A
Analog input (differential)	$V_{in,+} - V_{in,-}$	+10 V – -10 V

Table 3.2 – Characteristics of the Escon 50/5 motor driver^[9;12].

Basically, the working principle of such a driver is the following. It homes an analog input receiving a differential signal between -10 V and 10 V from the microcontroller. It then converts this signal into a proportional current to be provided to the motor. However, since it has been chosen to work with an Arduino DUE, the analog signal used to command the motor could only vary between 0.55 V and 2.75 V, what is far from the initial input voltage range of the Escon. One possibility to overcome this issue was to introduce electronic components to convert this into the required voltage range. Another possibility was to rely on an interesting feature of most of the Escon drivers, being that there are programmable. This programmable aspect means that it is possible to modify the input voltage range of the Escon 50/5 to make it correspond to the Arduino signals, i.e. for example delivering an output of 0 A for an input of 0.55 V and 15 A³ for an input of 2.75 V. This programmable aspect has allowed avoiding the use of transition electronics. One drawback of this configuration would be a possible loss of resolution.



Figure 3.3 – Escon 50/5 motor driver^[9].

As indicated in Table 3.2, the Escon 50/5 could potentially be fed with 50 V. However, a power supply of 24 V has been chosen since the motor is a 24 V model⁴. It has been programmed to deliver current from -0.652 A to 0.652 A (nominal current of the motor) for differential input voltage varying from 0.55 V to 2.75 V. Its analog input has a 12-bit resolution. That means that if the Escon 50/5 received a differential signal between -10V and 10 V, the resolution regarding the delivered current would be of 0.32 mA. When changing the differential input voltage range to 0.55 V-2.75 V, only 450 of the initially

³15A is the maximal current that can be delivered by the Escon 50/5 only for durations of less than 20 seconds.

⁴Actually, due to losses, the 24 V are not directly applied to the motor and the Escon could therefore be fed with slightly more than 24 V.

available 4096 bits are used. A variation of 1 bit leads now to a variation of 2.89 mA. One order of magnitude in resolution was thus lost but this did not impact the system since the motor works at higher current than mA range.

3.3 Sensors

Sensors are required to measure the different variables that need to be controlled. Since control algorithms are based on sensors measurements, a proper selection of sensors is crucial to achieve good performances. In the case of the centrifugal ring positioner where the aim is to control the position of the mobile on the rod, a position sensor was needed. As further detailed in Section 4, it has been decided to implement a cascade control for this system. As discussed in the state of the art, cascade control implies the implementation of an additional control loop which aims for this system to control motor velocity. An angular velocity sensor was therefore also required in addition of the position sensor for the mobile.

3.3.1 Position sensor

There exists plenty of position sensors with different working principles (resistive, Hall effect based, optical, ultrasonic, capacitive...). The research of the position sensor for the centrifugal ring positioner has started by investigating the sensors reported in the state of the art for existing didactic devices such as the inverted pendulum and the ball and beam. It has been previously reported that potentiometer as well as ultrasonic sensors could be potential convenient solutions. However, in the ball and beam, the potentiometer sensing is based on the contact of the ball with the beam. Using this kind of measurement device would have implied constraints (shape, material...) on the design of the system, both for the mobile and for the arm. As further explained in Section 3.4.2, we wanted to keep the system design relatively simple. Therefore, potentiometers have been disregarded. Ultrasonic (US) sensors are contactless and therefore imply much less constraints regarding the mobile and the system design. Infrared (IR) sensors, used in the SAAS department for application such as the ball and beam or the ball in the tube⁵ also present this advantage. Both sensor types were thus potential candidates for the centrifugal ring controller.

From this discussion, two sensor models have emerged: the Sharp GP2Y0A41SK0F and the HC-SR04. The first one is an optical infrared sensor while the second one is an ultrasonic sensor. The main characteristics of these two sensors are listed in the Table 3.3.

⁵The ball in the tube in another didactic control system which aim is to control the height of a ball inside a tube by acting on a fan.

	SHARP GP2Y0A41SK0F	HC-SR04
Technology	Infrared	Ultrasonic
Supply voltage Vcc	5 V	5 V
Operating current	12 mA	15 mA
Type of output	Analog	Digital
Measuring range	4-30 cm	2-400 cm
Short measuring cycle	16.5 ms	50 ms
Dimension	44.5 × 18.9 × 15.5 mm	45 × 20 × 15 mm
Weight	3.6 g	8.5 g
Picture	 Picture from [13].	 Picture from [14].

Table 3.3 – Comparative table between the IR Sharp GP2Y0A41SK0F and the US HC-SR04^[13;14].

For several of the characteristics, both sensors are relatively similar. They are both fed by a 5 V voltage that can be supplied by the Arduino, operate at small current and are small and light. However, several elements have orientated the choice towards the infrared sensor. Firstly, since the length of the rod is about 20 to 30 cm (see Section 3.4.2), the measuring range of the infrared sensor is much more adapted for the centrifugal ring positioner than the one of the ultrasonic sensor. Secondly, it is noteworthy that both sensors present a short measuring time, corresponding to the minimal duration between two consecutive measurements. This represents a non-negligible dead-time in the system dynamics. As small as possible short measuring time are therefore sought for sensors. Finally, the noises introduced by the slip ring (see Section 3.5) could hinder the proper detection of the ultrasonic echo signal. This would therefore not allow to obtain high quality ring position measurements with the ultrasonic sensor. For these reasons, the Sharp model has been selected for the centrifugal ring positioner.

From the datasheet of the Sharp GP2Y0A41SK0F, it is possible to linearise the measure characteristic by plotting the output voltage as a function of the inverse of the distance. This characteristic has been derived from the centrifugal ring positioner sensor and is represented on Figure 3.4.

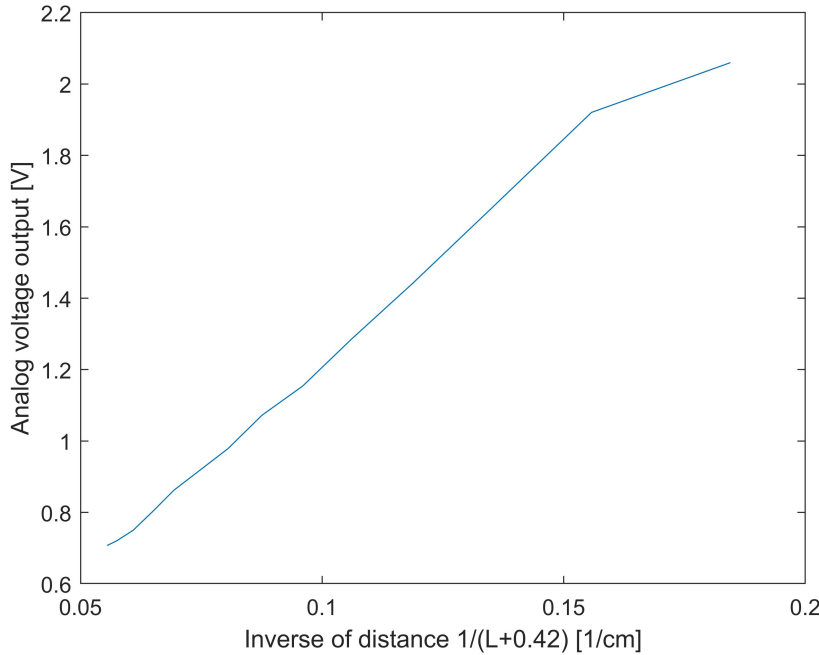


Figure 3.4 – Output distance characteristics with the inverse of distance of the Sharp GP2Y0A41SK0F.

3.3.2 Angular velocity sensor

Different sensors can be used to measure a motor angular velocity. There exists two classes of angular velocity sensors, those which measure directly the velocity and those which measure the angular position. In the latter case, the velocity has therefore to be numerically derived. Sensors such as the ones cited in the state of the art for the inverted pendulum and for the ball and beam, namely rotary potentiometer and encoder, belong to the second class. As cited in Section 3.2.1, the motor that has been chosen was already coupled a three channels optical incremental encoder, the HEDS 5540. It has been decided to start with this velocity sensor since it is part of the recommended sensors found in the Maxon catalogue for the selected motor. This encoder is shown on Figure 3.5 and its relevant characteristics are listed in Table 3.4.



HEDS 5540	
Supply voltage	5 V
Count Per Turn (CPR)	500
Maximum velocity	12000 rpm

Figure 3.5 – HEDS 5540 Encoder^[10]. **Table 3.4** – Characteristics of the HEDS 5540 encoder^[12].

As discussed previously, an encoder measures the angular position of a motor. An encoder such as the HEDS 5540 has an output consisting of two square waves in quadrature^[12]. The CPR corresponds to the number of rising edge of one of the square waves per turn. This encoder has a CPR of 500, which means that for one rotation of the gearmotor (gear reduction shaft side), the encoder emits 17500 counts ($CPR \times \eta_g$). The resolution of the encoder has been multiplied by 4 by measuring the rising edge of the outer waves and both failing edges. By doing that, one rotation of the gearmotor shaft leads to 70000 counts

and a resolution of 0.005° of the gearmotor shaft has been obtained. To obtain the angular velocity, the change in angular position during a precise time interval was calculated.

3.4 Design of the system

Regarding the design of the system, the only available literature was the project report cited in the state of the art^[6]. This report mainly focuses on simulations and does not detail the system design apart from some numerical values. The choice of the precise design of the centrifugal ring positioner implemented in this thesis was therefore quite flexible but the general design ideas originated from the system represented on Figure 1.8. Before constructing the system, a three-dimensional model was realised with the software Solidworks. This model is represented on Figure 3.6. Most of the pieces intervening in the system have been 3D printed using Poly-Lactic Acid (PLA) as material.

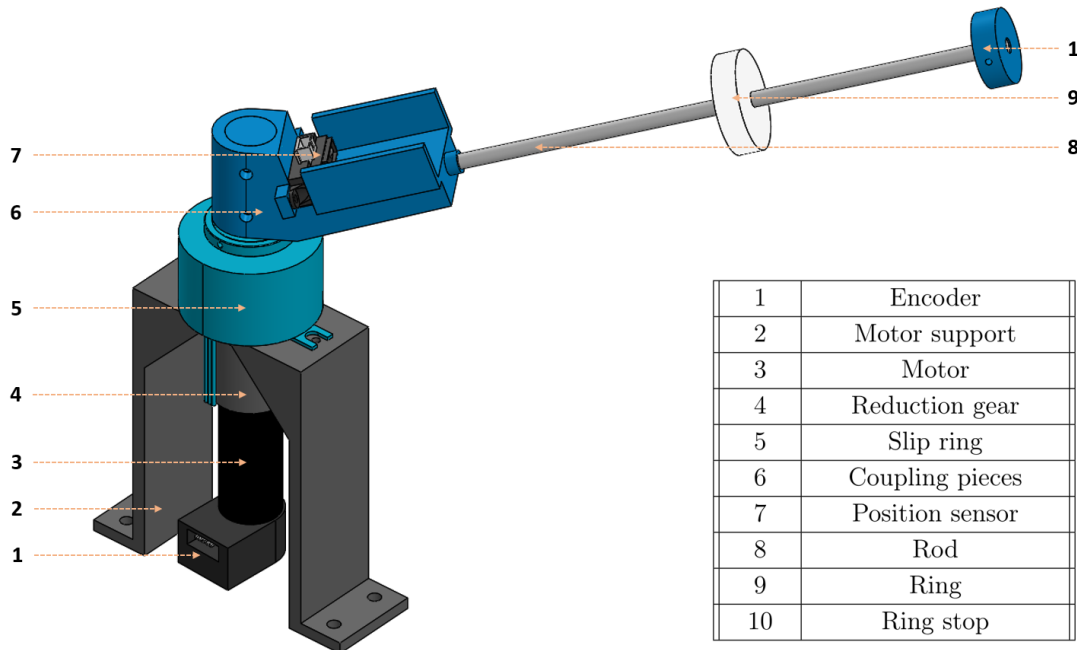


Figure 3.6 – Three-dimensional model of the centrifugal ring position (realised on Solidworks).

3.4.1 Motor support

The encoder below the gearmotor is not intended to support the weight of the overall system. For this reason, a piece called support motor was designed (Figure 3.7). This piece consists of the only connection between the system and the ground. It contains a large hole in its middle to incorporate the motor shaft. Around this hole are located four screw holes aiming to carry the gearmotor. This piece also aims to carry and fix the stationary part of the slip ring. To increase the mechanical resistance of the support, diagonal reinforcements have been added.

3.4.2 Mobile ring and rod

Regarding this part of the design, since no relevant literature was available, our aim was to keep things simple. The simplicity of implementation was therefore an important criterion for the choice of the design and components.

Concerning the mobile, different geometries have been envisaged such as spherical or cylindrical. The choice of the mobile shape is directly linked to the mobile motion on the tilted arm. A preliminary idea was to consider a ball inside a tube in the same idea of the ball in the tube benchmark. However, this would have strongly constrained the choice of material and geometry of the arm. Indeed, to illustrate control theory principles, it is more appropriate to be able to see the mobile moving. The tube should therefore be transparent or designed with openings in such a way that the ball can be seen. Procuring a ball of the desired dimension in the desired material would probably have in addition required reaching out manufacturers. Once the ball delivered by the supplier, no further significant changes would have been possible. Moreover, the spherical shape of a ball might lead to some position measurements issues.

To keep things simple, it has been decided to use a hollow cylindrical mobile, the so-called ring, sliding on a rod. This configuration allows a good visual representation of the ring position and a simple system construction. Moreover, the cylindrical form of the mobile allowed to use the 3D-printer available in the SAAS department to make tests for mobile parameters such as dimension and weight. Note that we could have considered a rail to make the cylinder slide with low friction but again, this would have added complexity in the design and construction.

Aluminium was chosen as material for the rod due to its stiffness and its lightness. A relatively small rod diameter of 6 mm has been chosen to limit contact area with the mobile and hence limit friction. The rod length has been chosen to be between 20 cm and 30 cm to keep the system compact. At the end of the rod, a stop piece also 3D-printed has been fixed with a clamping screw. Regarding the mobile, its cylindrical form provides symmetry. The initial idea was to use a mobile in Teflon to benefit from its low friction coefficient. However, this presents the drawbacks that it is quite expensive and it must be processed, what can take time. For this reason, before processing the final ring in Teflon, several 3D-printed prototypes with different hole dimensions and hole diameters have been tested to find the optimal sliding conditions on the rod. It has been concluded that best sliding conditions were obtained for an inner diameters of 6.3 mm and that to avoid external disturbances in the measurements, the ring diameter must be higher than 4 cm. Hence, the final ring external diameter is 5 cm (Figure 3.8). Since acceptable control results have been obtained with the 3D-printed mobile, it has been decided not to switch towards Teflon mobile. An additional advantage of 3D-printing is that we could play on the density of the mobile by playing on the filling conditions.

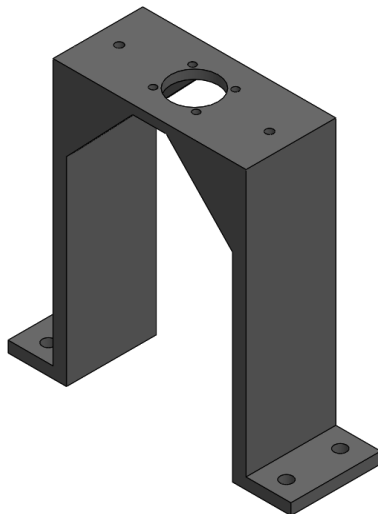


Figure 3.7 – Three-dimensional model of the motor support (designed on Solidworks).

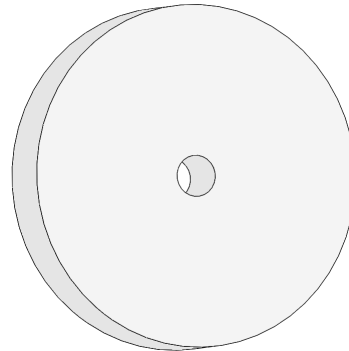


Figure 3.8 – Three-dimensional model of the ring (designed on Solidworks).

3.4.3 Coupling pieces

The tilted rod has to be coupled to the shaft of the motor. This is the aim of the two coupling pieces, the motor coupling and the rod coupling.

The motor coupling (Figure 3.9) consists of a cylinder that is fixed to the motor shaft with a clamping screw on its bottom side. It contains two holes on its upper part to fix the rod coupling piece with screws. The motor coupling is relatively long since there must be enough space between the motor and the rod coupling to place the slip ring.

The rod coupling (Figure 3.10) has a much more complex geometry. It contains a large cylindrical hole on one side to insert the motor coupling piece. On its other side, it contains a smaller cylindrical tube in which the rod can be inserted and fixed from below with two clamping screws. Before constructing the system, different values of the tilt angle of the rod have been investigated through control simulations. It appeared from these simulations that a rod angle of 20° leads to motor angular velocities and torques fully compatible with the selected gearmotor. The selection of this angle value was supported by the one found in the project report^[6], also being 20° . This rod coupling piece also contains a specific place to fix the position sensor. A sensor hosting seat and walls have been added on each side of the piece after performing experiments with the sensor. It has indeed been observed that these structure improvements allow to decrease external measurement disturbances. It has been decided to begin with a fixed tilt angle for the rod coupling piece. An interesting feature that could be implemented on a future centrifugal ring positioner would be a rod coupling piece with modifiable tilt angle, leading to more challenging control of the system.



Figure 3.9 – Three-dimensional model of the motor coupling piece (designed on Solidworks).

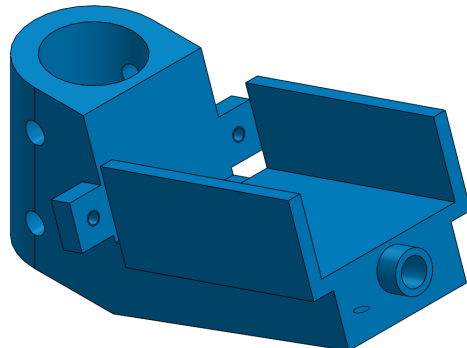


Figure 3.10 – Three-dimensional model of the rod coupling piece (designed on Solidworks).

3.4.4 Slip ring

The slip ring is an essential component of the centrifugal ring positioner. Indeed, wires of the position sensor need to be connected to the Arduino. Since the part of the system containing the microcontroller is stationary and the part containing the sensor is rotating, an element is needed to make the electrical connection between both parts. This element is the slip ring. It is constituted by a non-rotating bottom part and by a rotating upper part. For the centrifugal ring positioner, the bottom part is fixed to the motor support while the upper part is connected to the motor shaft. Therefore, the bottom part contains fixed wires while the upper part contains wires rotating at the speed of the system. Figure 3.11 shows the need of a slip ring for an application such as the centrifugal ring controller.

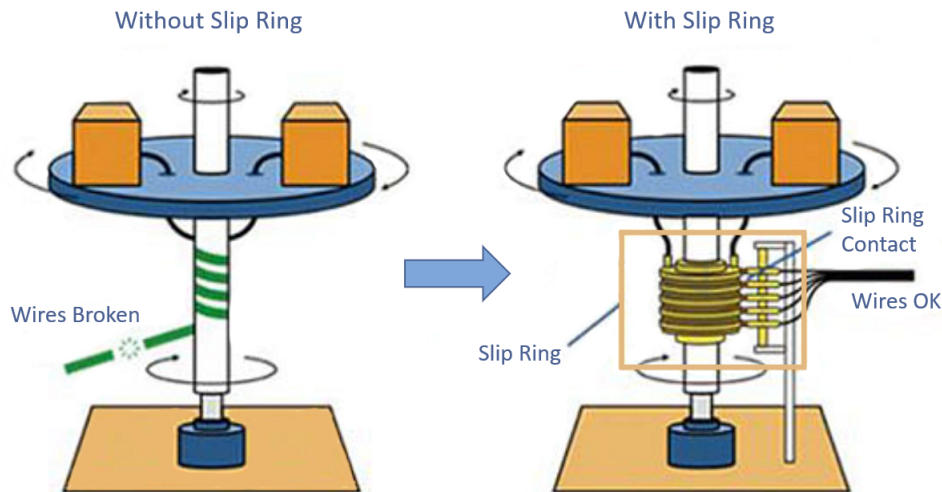


Figure 3.11 – Illustration of the working principle of a slip ring (adapted from^[11]).

Different models of slip rings exist. For our application, we opted for a hollow cylindrical model allowing to be fixed around the motor shaft. The chosen hole dimension was 20mm since the motor coupling piece has a diameter of 20mm. Specialised slip rings suppliers have been contacted in order to acquire this component. Table 3.5 provides the characteristics of the two most relevant slip ring models found.

	SENRING H2056-0610	MOFLON MT2042-S03
Hole diameter	20 mm	20 mm
Outer diameter	56 mm	42 mm
Height	40 mm	31.4 mm
Wires	6 @ 10A	3 @ 5A
Voltage range	0-600 V	0-240 V
Maximum speed	250 rpm	150 rpm
Lifetime	20 million revol.	15 million revol.
Price (pc. + shipping)	90 (55 + 35) USD	175 (115 + 60) USD
Lead time	Stock	10 days
Shipping time	3 to 5 days	3 days
Picture	 Picture from [11].	 Picture from [15].

Table 3.5 – Comparative table between the Senring H2056-0610 and the Moflon MT2042-S03 slip rings^[11;15].

Regarding their sizes, both models are more or less equivalent even though the Moflon model is slightly smaller. The Sharp position sensors has three wires that have to be connected to the arduino. In any case, current of the order of several amperes will flow in these wires. Both slip rings are therefore convenient in term of connection wires. However, if for one reason, the Sharp sensor is one day replaced by another position sensor requiring more than three connections to the arduino, the Moflon slip ring would not be appropriate. The Senring model also has a higher maximal rotational velocity and a higher life time than the Moflon model. It is in addition half the price of the Moflon and was directly available when ordering while the Moflon model had a longer lead time. For all these reasons, it has been decided to opt for the Senring H2056-0610 slip ring.

3.5 Improvement of the position sensor signal

During the first experiments performed with the position sensor, it was noticed that the rotation of the slip ring strongly affects the measurements of the sensor. To illustrate that, Figure 3.12 shows sensor outputs first with the system fixed, then with the system rotating. In both cases, the ring was placed in the same position.

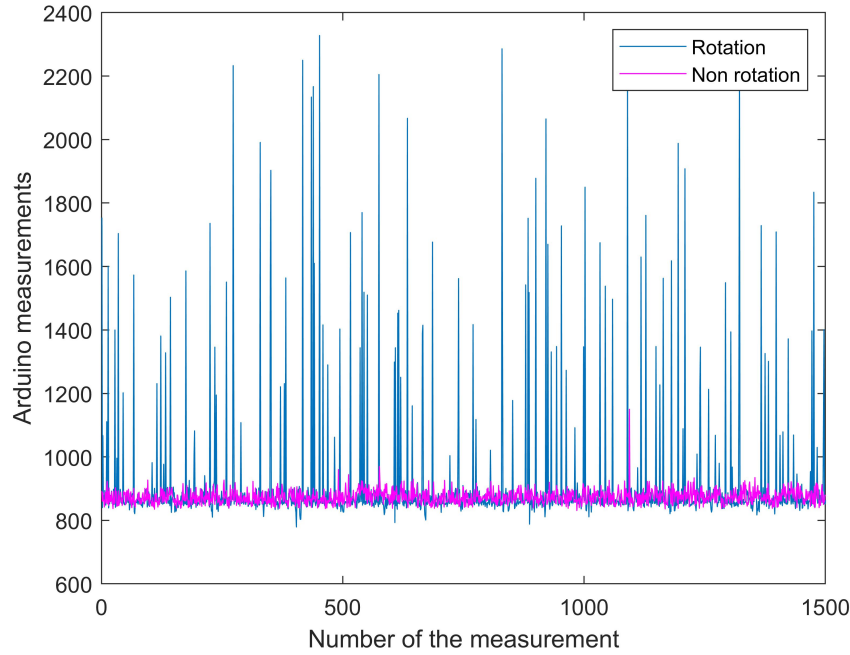


Figure 3.12 – Noises in the position sensor signal due to the slip ring rotation (Arduino measurement corresponds to the sensor output voltage multiplied by 4096/3.3).

As clearly showed by Figure 3.12, the rotation of the slip ring causes strong fluctuations in the sensor output signal. By not taking any measures against that, no proper control of the ring position would have been possible. It has been assumed that these noises in the signal were due to contact failures inside the slip ring caused by vibrations due to the rotation.

The first measure that has been taken assumes that the fluctuations in the sensor output are due to some loss of energy supply (V_{cc}) due to the contact failures. A capacitor, playing the role of a back-up energy source has therefore been placed on the sensor supply wire, between the slip ring and the sensor.

The second implemented measure assumes that using more than one connection of the slip ring to carry each signal would allow to lower the noises. Instead of using only three of the six available connections (for the supply voltage, for the ground and for the output voltage) of the slip ring, all of them were used, meaning that each signal passes through two connections. If there is a loss of contact for one connection, the signal would still be transmitted via the second one.

Finally, a capacitor has been placed on the output voltage of the sensor after that the signal passes through the slip ring, aiming at filtering high signal frequencies. The value of the capacitor has been carefully selected. Indeed, the higher the capacitor, the higher the filtering ability. However, this capacitor also introduces a phase shift in the signal, which has a destabilising effect. The selection of the capacitor has thus been performed through experiments. Table 3.6 shows the standard deviations of a series of ring position measures obtained during system rotation with different capacitors.

Capacitor value	Standard deviations (Arduino measurements)
No (system fixed)	21
No (system rotating)	188
$10nF$	15
$22nF$	13
$47nF$	12
$100nF$	12
$330nF$	3

Table 3.6 – Standard deviations of the position sensor signal for different capacitor values.

From Table 3.6, it is clear that the 330 nF capacitor presents the best filtering ability. This capacitor has been chosen after verifying it does not impact the ring dynamics measurements.

3.6 Wiring diagram

This section contains some explanations about wiring connections between all the previously discussed elements. The overall wiring diagram of the centrifugal ring positioner is illustrated on Figure 3.13.

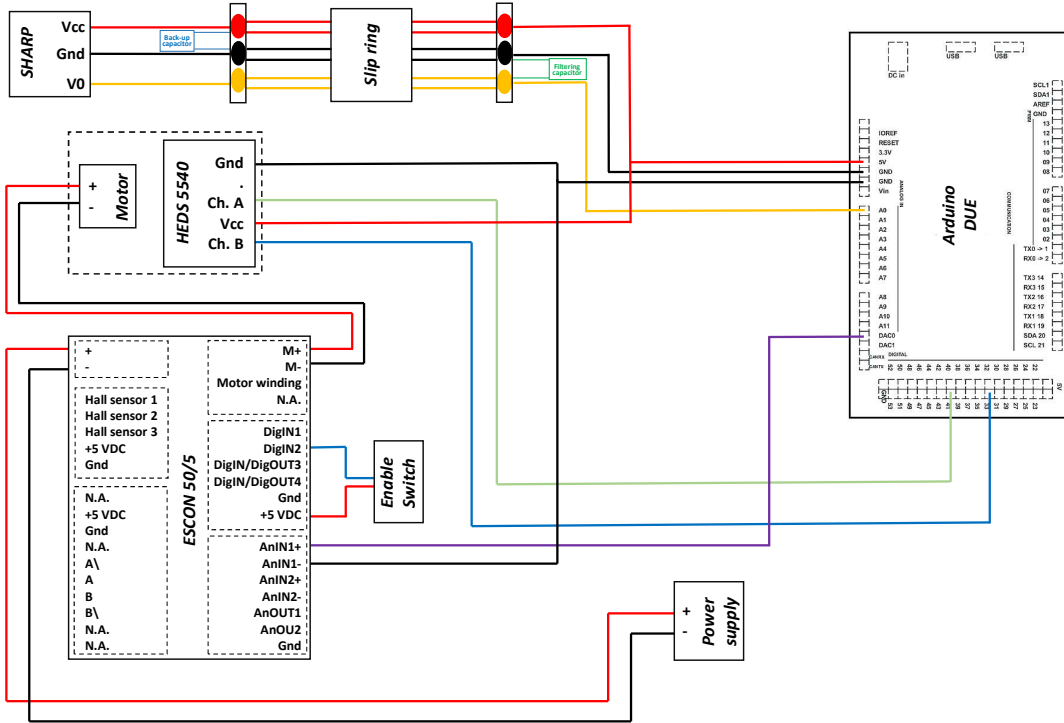


Figure 3.13 – Wiring diagram of the centrifugal ring positioner.

The main elements of this wiring diagram are the following:

- The Escon motor driver receives power from the power supply.
- The Escon motor driver is driven by a digital to analog output of the Arduino.

- Both sensors (position and angular velocity) are supplied by the 5V output of the Arduino.
- The position sensor output is connected to an analog input of the Arduino.
- Both encoder outputs are connected to digital inputs of the Arduino.

3.7 Final system

Figure 3.14 shows the final centrifugal ring positioner built during this master thesis. All the selected elements such as the microcontroller, the motor driver and the power supply are represented on the picture.

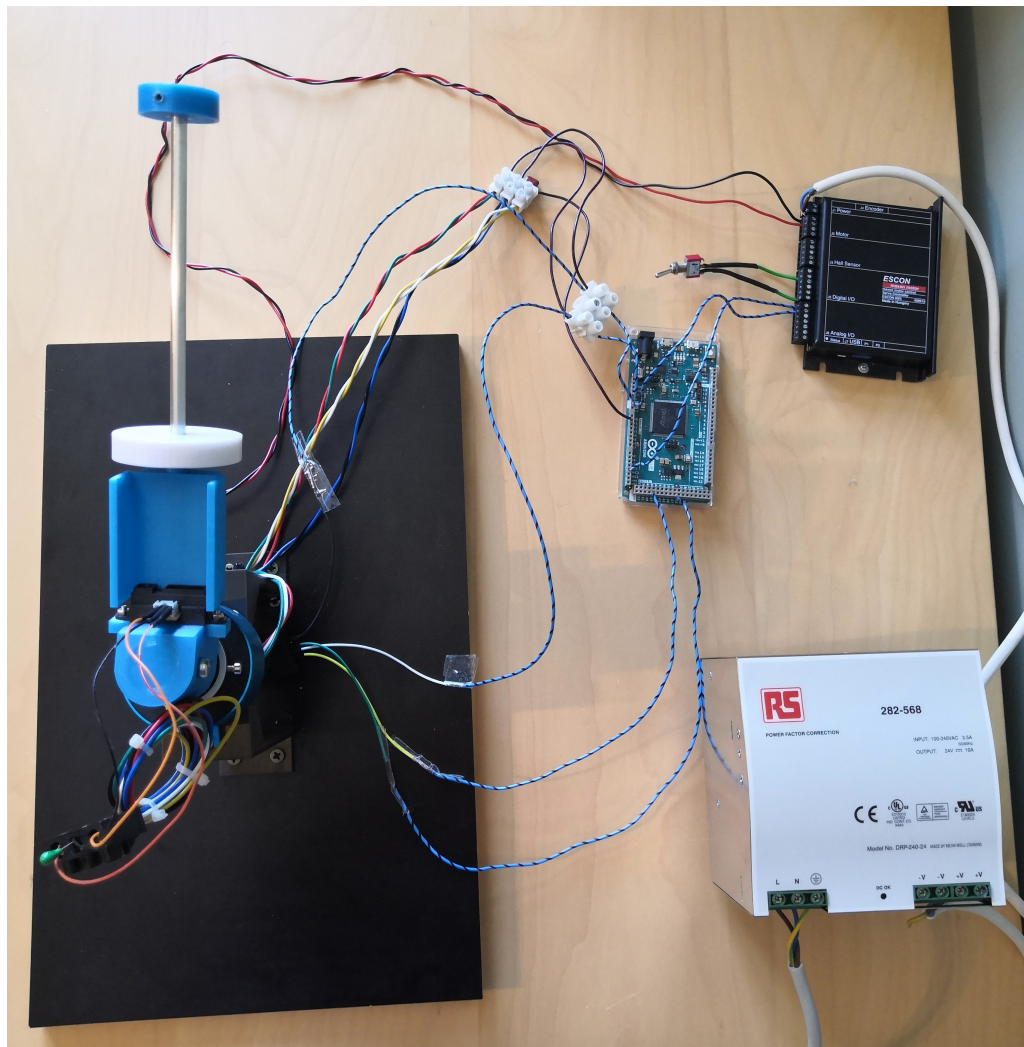


Figure 3.14 – Top view picture of the centrifugal ring positioner.

Figure 3.15 represents a picture of the system itself in which all the previously discussed pieces can be seen.

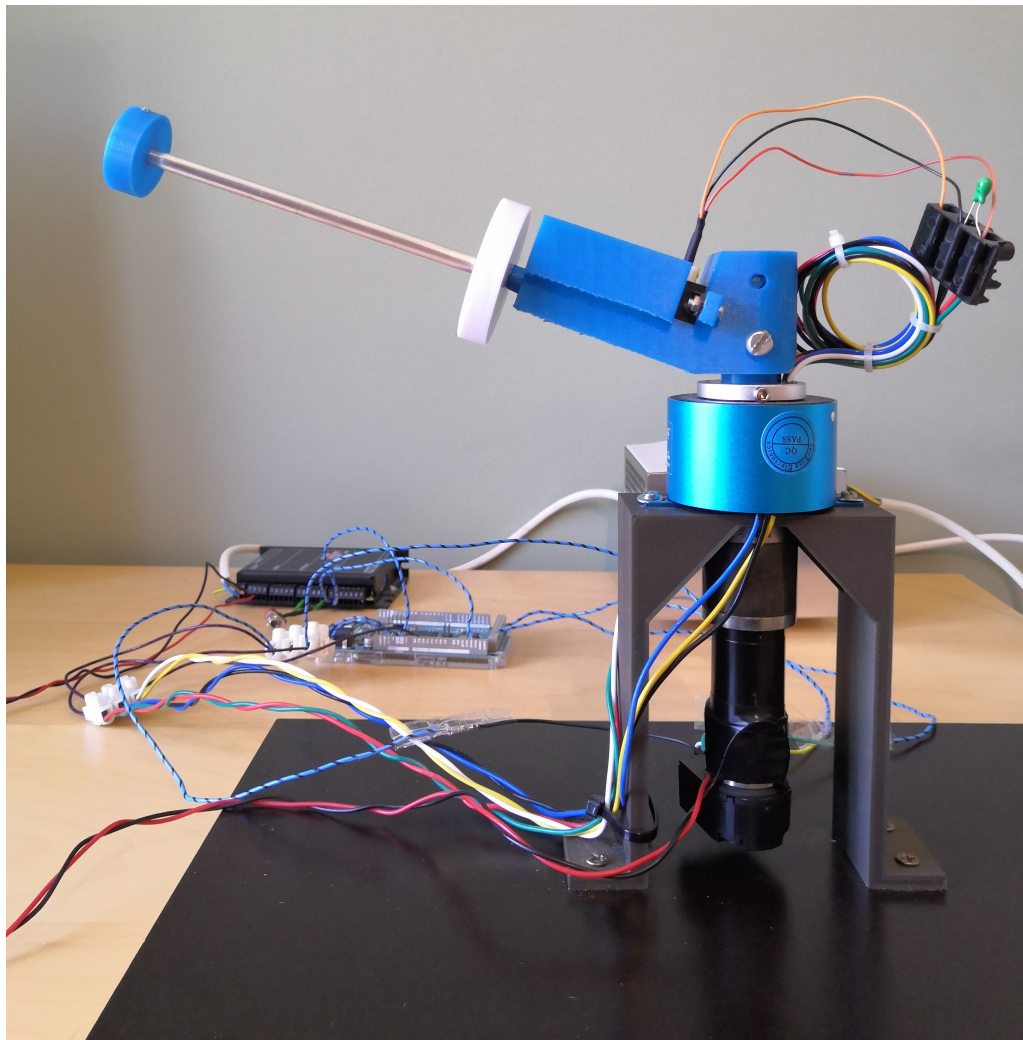


Figure 3.15 – Profile view picture of the centrifugal ring positioner.

Chapter 4

Control of the centrifugal ring positioner

This section details the control of the centrifugal ring positioner. It starts by developing cascade control, the control strategy that has been applied on the system. Then, the way of obtaining the transfer functions required for such a strategy is developed. Thereafter, the inner loop control is discussed, starting from the design of the controller through the real device implementation. Finally, the design of the outer loop controller as well as ring position simulation and real device experiments are considered. The Simulink model used for the simulations of the ring position control are reported in Appendix D.

Since this section addresses the control of the centrifugal ring positioner, it is worth mentioning the basic control requirements of such a system. The first one consists of the setpoint tracking of the ring position while the second one regards the robustness of the system. In order to keep a certain margin from instability, usual values of gain and phase margins that are sought in closed-loop systems are at least 6 dB for the gain margin and between 30° and 60° for the phase margin. Obtaining such stability margins consists of the second control requirement.

4.1 Control strategy

Regarding the control of the centrifugal ring positioner, it has been decided to implement a cascade control strategy. Cascade control has already been discussed in the state of the art, but let us remind ourselves the main features and advantages of this control strategy. Cascade control consists in dividing the centrifugal ring positioner into two subsystems and in implementing a control loop for each of them. The inner loop consists of the control of the motor angular velocity while the outer loop consists of the control of the ring position. This strategy improves the system dynamics by lowering the effect of disturbances at the motor level on the ring position. An important requirement of cascade control is that the inner loop must have a faster response than the outer loop. This is indeed respected since the motor presents a faster dynamics than the ring. The main disturbance that is encountered within the inner loop is friction.

Figure 4.1 shows the cascade control block diagram of the centrifugal ring positioner. The transfer functions involved in this diagram are listed in Table 4.1.

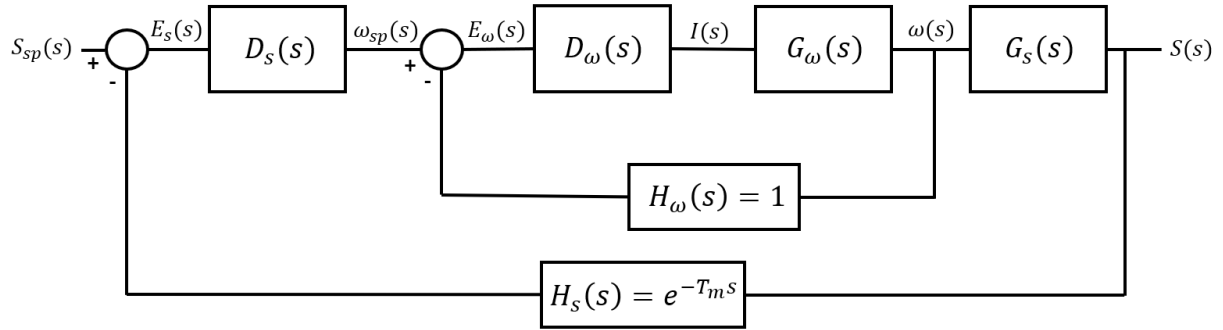


Figure 4.1 – Cascade control block diagram of the centrifugal ring positioner.

Ring position-motor angular velocity	$G_s(s) = \frac{S(s)}{\omega(s)}$
Ring position controller	$D_s(s) = \frac{\omega_{sp}(s)}{E_s(s)}$
Ring position sensor	$H_s(s) = e^{-T_m s}$
Motor angular velocity-motor current	$G_\omega(s) = \frac{\omega(s)}{I(s)}$
Motor angular velocity controller	$D_\omega(s) = \frac{I(s)}{E_\omega(s)}$
Motor angular velocity sensor	$H_\omega(s) = 1$

Table 4.1 – Centrifugal ring positioner transfer functions.

Both motor angular velocity and ring position sensors were assumed to have a unitary transfer function. However, as indicated in Table 3.3, the position sensor presents a short measuring cycle of 16.5 ms. This means that the measurement presents a dead time of 16.5 ms, indicated as T_m , representing a period during which the outer controller can not act on the ring position. It was therefore crucial to take this dead time into account for the position controller design.

4.2 Identification of the system transfer functions

4.2.1 Linearised system dynamics

A state-space representation of the centrifugal ring positioner dynamics has been derived in Section 2.3. This is represented in equation 4.1.

$$\begin{cases} \dot{x}_1 = x_2 \\ \dot{x}_2 = \bar{x}_3^2 \cos^2 \theta x_1 - \frac{c}{m} x_2 + 2\bar{x}_1\bar{x}_3 \cos^2 \theta x_3 \\ \dot{x}_3 = -\frac{2m\bar{x}_1\bar{x}_3 \cos^2 \theta}{(i_{33} + m\bar{x}_1^2 \cos^2 \theta)} x_2 - \frac{f}{(i_{33} + m\bar{x}_1^2 \cos^2 \theta)} x_3 + \frac{K}{(i_{33} + m\bar{x}_1^2 \cos^2 \theta)} u \end{cases} \quad (4.1)$$

with

$$x = \begin{cases} x_1 = \delta s \\ x_2 = \delta \dot{s} \\ x_3 = \delta \omega \end{cases} \quad \bar{x} = \begin{cases} \bar{x}_1 = \bar{s} \\ \bar{x}_2 = \bar{\dot{s}} \\ \bar{x}_3 = \bar{\omega} \end{cases} \quad u = \delta i$$

Theoretically, this state-space representation would allow to obtain both $G_\omega(s)$ and $G_s(s)$ transfer functions. However, using this mathematical model to obtain the transfer function between the input current and the motor velocity would not be the most appropriate way to operate. Indeed, this model involves motor friction parameters such as C_r and f that are not trivial to quantify. One way to obtain a more realistic model of the motor is to consider it as a black box model.

The system dynamics model above involves the motor angular velocity ω . However, as discussed in Section 3.2.1, the selected motor was a gearmotor. From now, the term "motor velocity" is considered for the system angular velocity, i.e. for the real motor velocity reduced from the reduction gear factor. In addition, for all the experiments and simulations that have been performed in the following sections, the rotating arm with the ring was already coupled to the gearmotor.

4.2.2 Transfer function of the motor

Considering the motor as a black-box consists in analysing the motor output for a specific input. This method was used to derive a transfer function for the gearmotor¹ by applying a step change in the input current in order to obtain a step response for its angular velocity. To fit a transfer function to these experimental data, a first order model was assumed and the optimal parameters in the least squares sense were determined.

The experimental step response as well as the identified model step response are represented on Figure 4.2.

¹Since the rotating arm was coupled to the motor during this experiment, this transfer function accounts for the inertia of the rod and the ring in addition to the one of the gearbox.

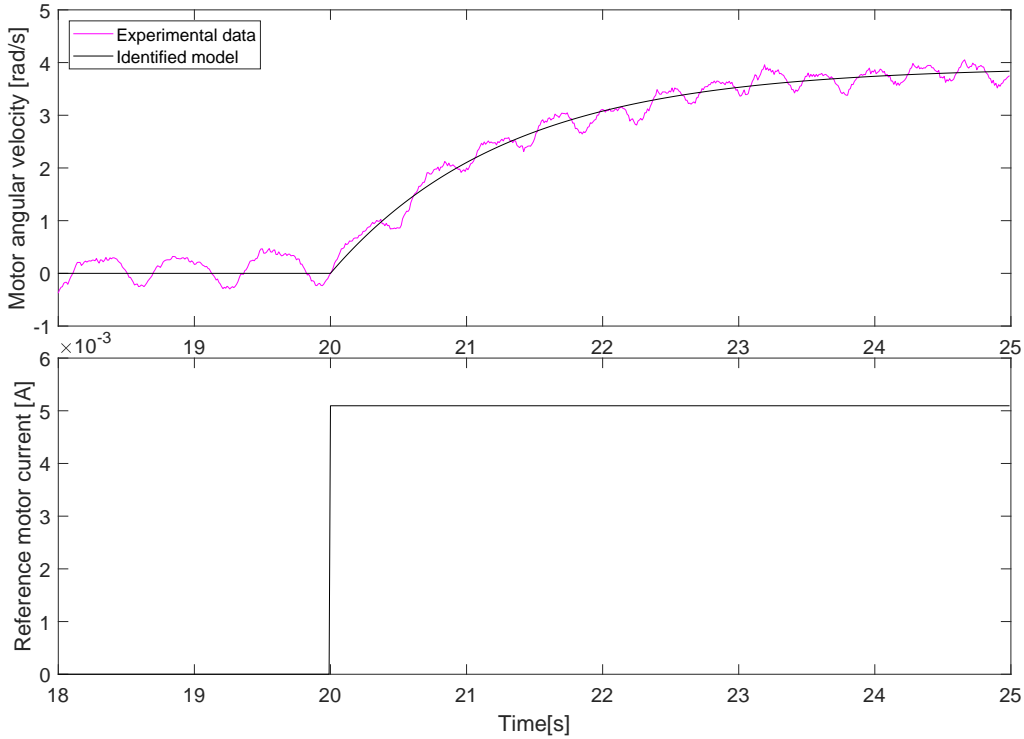


Figure 4.2 – Black-box motor model identification experiment.

The oscillations observed on the experimental step response are due to friction induced by the slip ring rotation. Based on this black-box model experiment, the motor transfer function has been identified. It is given by equation 4.2.

$$G_\omega(s) = \frac{\omega(s)}{I(s)} = \frac{769.4}{1.3s + 1} \quad (4.2)$$

4.2.3 Transfer function of the angular velocity-ring position subsystem

Since the subsystem between the motor angular velocity and the ring position is unstable, performing the same kind of experiment as for the motor to obtain this transfer function was not feasible. This transfer function was thus derived from the mathematical modelling of the system dynamics, especially from the second equation of the system 4.1. It is given by equation 4.3. The numerical values of the parameters involved in this transfer function are given in Table 4.2.

$$G_s(s) = \frac{S(s)}{\omega(s)} = \frac{2\bar{s}\bar{\omega} \cos^2 \theta}{s^2 + \frac{c}{m}s - \bar{\omega}^2 \cos^2 \theta} = \frac{0.97}{s^2 + 12.55s - 41.94} \quad (4.3)$$

Parameters		
Ring mass	m	0.0239 kg
Equilibrium ring position	\bar{s}	0.08 m
Equilibrium motor angular velocity	$\bar{\omega}$	6.89 rad/s
Rod tilt angle	θ	20°
Ring viscous friction coefficient	c	0.3 kg/s

Table 4.2 – Numerical values of position transfer function parameters.

Since this transfer function has been derived from the linearised system dynamics, it involves an equilibrium point. The minimal ring position of the rod, namely $\bar{s} = 0.08\text{ m}$, has been chosen as equilibrium position. Indeed, since the system must be brought close to its equilibrium point before starting the control, this ring position seems to be the most evident choice from a practical standpoint. The corresponding equilibrium angular velocity is $\bar{\omega} = 6.89\text{ rad/s}$. The ring viscous friction coefficient is also involved in this transfer function. Such friction data were not available, its value has thus been determined experimentally. The detailed determination of this coefficient is performed in Appendix B.

4.3 Inner loop: control of the motor angular velocity

Before designing the controller for the inner loop, it was relevant to consider an aspect related to the motor, especially to the reduction gear. Within the reduction gear, the gear teethes are spaced in order to allow a smooth rotation between two gears. When a change in direction of rotation occurs, the gear teethes suddenly hit against each other, leading to a shock. This phenomenon is called backlash. For the centrifugal ring controller, the gearmotor is likely to be submitted to sudden velocity setpoint variations, leading to backlash. Shocks and vibrations due to this backlash can negatively affect the position control. It was therefore important to keep in mind that the motor must not be submitted to sudden setpoint variation to limit gear jolt. Another important element is that sudden velocity variation will cause gear teethes wear, that will increase the dead zone and increase backlash in the long term.

Design of the inner loop controller

The design of both controllers was performed by first analysing root locus in continuous-time case. The continuous-time controller was thereafter approached by the discrete-time compensator by accounting for the digital implementation of the controller through the addition of a dead time in the loop. Indeed, the digital implementation of a controller usually requires a Digital/Analog Converter (DAC) and might need an Analog/Digital Converter (ADC) if the sensor measurements consist of an analog signal. The effects of each of these converters are approached by a delay corresponding to a half-sampling period, leading to a total dead time of one sampling period. In addition to the ADC converter, the computation time is also considered through the first half-sampling period. The resulting destabilising impact was taken into account via Bode diagrams. In order to approach as well as possible the controller designed in continuous-time, it is beneficial to select a very small value of sampling period. For this reason, the sampling period has been chosen to be 1 ms. More details about the selection of the sampling period are given in section 4.4.1.

The aim of the inner loop controller is to accelerate the motor response to disturbances before they affect the ring position. Since the transfer function of the motor has been identified as a first order transfer function (equation 4.2), the motor could theoretically be controlled with a simple P controller. While this would lead to an offset with respect to its setpoint, it is not an issue since the main requirement for the inner loop is to be fast. Alternatively, using a PI controller would allow to cancel this offset but would significantly slow down the motor dynamics. Since a simple P controller already allowed to get sufficiently fast response, it has been decided to opt for this kind of controller. A PD controller could also have been envisaged if there were a significant need of increasing

further the inner loop bandwidth. The transfer function of the inner loop P controller is given by equation 4.4.

$$D_\omega(s) = k_p \quad (4.4)$$

The root locus of the motor transfer function coupled to a P controller is represented on Figure 4.3 and correspond to the negative part of the real axis located left to the system pole.

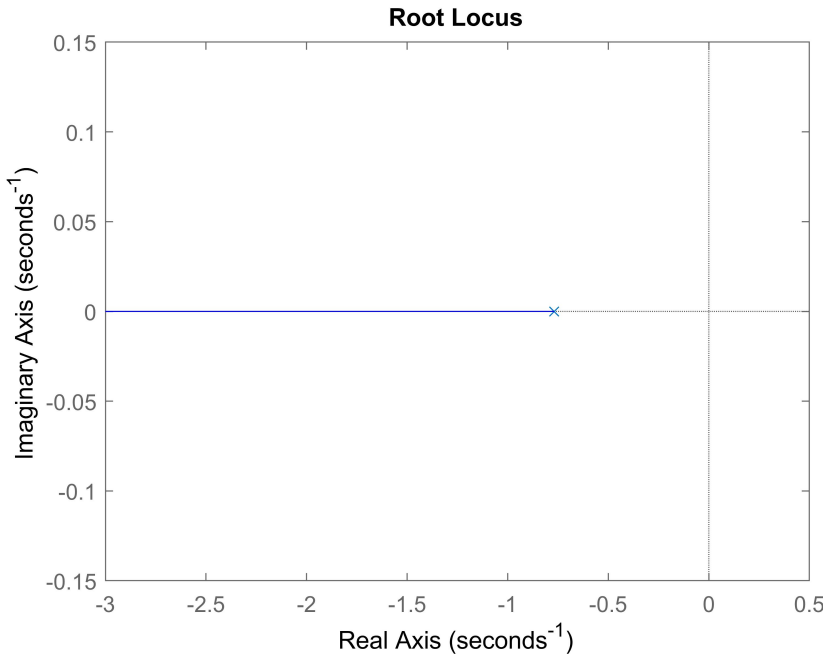


Figure 4.3 – Root locus of the motor transfer function coupled to a P controller.

This root locus showed that in continuous-time case, the gain k_p of the controller could freely be chosen in order to accelerate the inner loop dynamics. However, two important considerations must be kept in mind while selecting a value for k_p . First, as previously discussed, the dead time originating from the discrete implementation of the controller causes a decrease in stability margins for increasing k_p values. Secondly, high values of k_p might lead to actuator saturation. As a reminder of Section 3.2.2, the Escon motor driver has been programmed to deliver current in between -0.652 A and 0.652 A, meaning that if the controller command is out of this range, the actuator is not able to deliver the required current².

Since the inner loop control consists of a simple P controller, the discretization of the controller is not discussed here. A deeper discussion about the discretization of the outer loop controller is performed further in Section 4.4.1. The influence of the dead time introduced by the discrete controller was considered through Bode diagrams. Three values of controller gain k_p leading to highly robust inner loops have been selected. Their stability margins are listed in Table 4.3.

²It is noteworthy that during motor rotation, the counter-electromotive force is such that current saturation is reached for lower values than the nominal motor current.

k_p	Gain margin	Phase margin
0.05	34.5 dB	89.8°
0.15	25.0 dB	85.4°
0.5	14.5 dB	73.2°

Table 4.3 – Stability margins of the open inner loop.

The selection of the controller could not simply be made based on the stability margins. It must be kept in mind that an excessive value of k_p might lead to a non-physically realisable controller output. Moreover, the gearmotor backlash also represents a factor to consider in the controller selection. This will be more detailed further.

P controlled inner loop simulation

Control simulations of the inner loop have been run on Simulink with the values of k_p listed in Table 4.3. Since the motor is likely to be submitted to various setpoint changes due to variation of ring position, the selected angular velocity setpoint consisted in a positive step like change followed by a negative step like change.

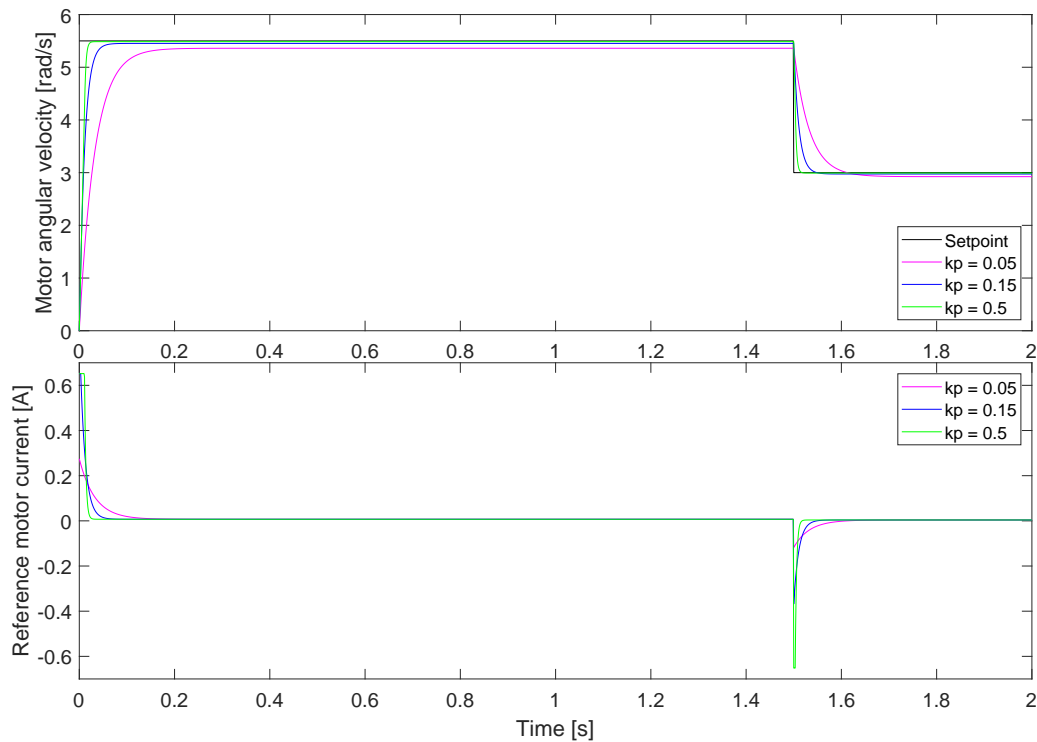


Figure 4.4 – Simulation of the motor angular velocity coupled to P controllers.

From Figure 4.4, the three values of k_p that have been tested all led to very fast responses to a sudden setpoint change. As expected, the higher the gain, the faster the response and the lower the offset with respect to the setpoint. However, the controller output, i.e. the reference motor input current, must be considered. For the initial step change, both commands for $k_p = 0.15$ and $k_p = 0.5$ reach the saturation limit, i.e. 0.652 A, since the amplitude of the step change is quite important. However, such a high step change in the velocity setpoint is not likely to be encountered for the centrifugal ring positioner cascade

control and this is therefore not problematic. Smaller step changes such as the negative one performed at 1.5 s in the simulation are more likely to occur. For $k_p = 0.5$, the current reaches its saturation limit while this is not the case for the smaller gain values. This simulation gave a first idea of the potential values of k_p that might be selected for the design of the outer loop controller, keeping in mind that choosing a too high value for k_p might lead to actuator saturation.

Implementation of the inner loop P controller

Even though it has been observed through simulations that actuator saturation can be reached in some cases, all of the three controllers discussed previously have been implemented on the motor of the centrifugal ring positioner. The aim of this experiment was to submit the motor to the same setpoint profile and to compare the results with the simulation. The results of this experiment are represented on Figure 4.5.

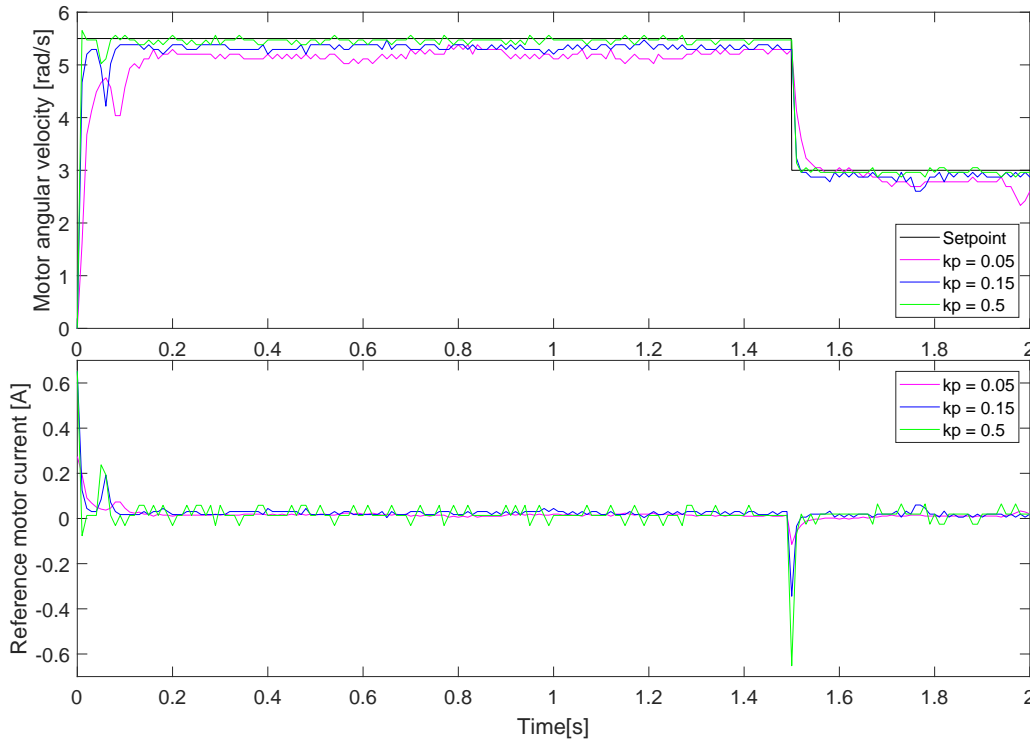


Figure 4.5 – Control of the motor angular velocity coupled to P controllers.

From Figure 4.5, the motor angular velocity can be properly controlled with the different P controllers discussed before. As in simulation, a higher gain leads to a faster response and to a lower offset compared to the setpoint. However, as discussed previously, an excessive gain could lead to saturation of the actuator, which is indeed observed for $k_p = 0.5$ at 1.5 s. Moreover, the gear reduction backlash is also a parameter that is involved in the selection of the controller gain in addition to the saturation. An important gain could cause sudden motor current variations leading to potential ring position control problems. The choice of the value of the gain could not be performed at this stage and had to be coupled with ring control experiments to observe the servomotor behaviour.

4.4 Outer loop: control of the ring position

By definition of cascade control, the output of the outer controller corresponds to the setpoint of the inner loop. Accounting for the inner closed loop previously designed with a P controller, a transfer function between the setpoint of the motor angular velocity and the ring position was derived. Indeed, the inner closed loop transfer function can be expressed as equation 4.5.

$$\frac{\omega(s)}{\omega_{sp}(s)} = \frac{D_\omega(s)G_\omega(s)}{1 + D_\omega(s)G_\omega(s)} = \frac{k_p G_\omega(s)}{1 + k_p G_\omega(s)} \quad (4.5)$$

Combining this transfer function in series with the one of the ring position (equation 4.3), the transfer function between the motor angular velocity setpoint and the ring position was obtained.

$$\frac{S(s)}{\omega_{sp}(s)} = \frac{\omega(s)}{\omega_{sp}(s)} \frac{S(s)}{\omega(s)} = \frac{k_p G_\omega(s)}{1 + k_p G_\omega(s)} \frac{2\bar{s}\bar{\omega} \cos^2 \theta}{s^2 + \frac{c}{m}s - \bar{\omega}^2 \cos^2 \theta} \quad (4.6)$$

This transfer function between the inner loop setpoint and the outer loop output was the basis of the design of the controller for the ring position.

With the aim of controlling the ring position, two different controllers have been designed and implemented on the system in order to compare their performances. These two controllers are a PID and a PD controller.

4.4.1 PID controller

Design of the outer loop PID controller

The outer loop controller aims at reaching the main control specification mentioned at the beginning of this section, i.e. controlling the ring position with respect to its setpoint. In addition, it must lead to a control system presenting the stated robustness criteria, namely a gain margin above 6 dB and a phase margin between 30° and 60°. In the same way it has been conducted for the inner loop, the design of the controller has started by analysing the root locus of the system transfer function (equation 4.6) coupled with the controller in continuous-time. Since dead times are not included in root locus³, Bode diagrams were thereafter used in order to account for dead times due to the discrete controller implementation and due to the position sensor.

In order to track the setpoint as well as possible, an integrator controller was desired to cancel any steady-state error during constant setpoint phases. By root locus analysis, it has been concluded that a PI controller was not sufficient to stabilise the outer loop. For this reason, a PID controller (equation 4.7) has been implemented.

$$D_s(s) = k \frac{(1 + sT_i)}{sT_i} \frac{(1 + sT_d)}{(1 + sT_f)} \quad (4.7)$$

with $T_f = T_d/N$.

³They could be introduced in root locus plot by using approximation such as Padé's approximation, but this has not been investigated.

Such a PID controller presents 4 parameters that can be selected to achieve the desired closed-loop performances. The value of T_d has been chosen so that the corresponding controller zero cancels the first negative pole of the system. The filtering time constant T_f is usually chosen to be 8 to 20 times faster than the time constant T_d . Despite the measures discussed in Section 3.5, the position sensor signal was still submitted to noise due to the rotation of the slip ring. To attenuate the effects of these disturbances, it was required to select a low value of N . For this reason, N has been chosen to be 8. Regarding the value of T_i , the choice was quite arbitrary, accounting for its influence of the system stability. The fourth PID controller parameter is the gain k , which value was chosen in order to achieve the desired ring position dynamics while respecting the stability margins (see further).

To design the controller, the parametric transfer function between the motor angular velocity setpoint and the ring position (equation 4.6) has been converted into a numerical one. To achieve that, in addition to the numerical values listed in Table 4.2, a value for the inner loop controller gain k_p was required. This gain is, in addition to T_i , T_d and T_f , an additional parameter that can be varied to modify the root locus of the outer loop. Figure 4.6 shows the root locus of the position transfer function coupled to the PID controller with the different values of k_p tested in the motor controller design section.

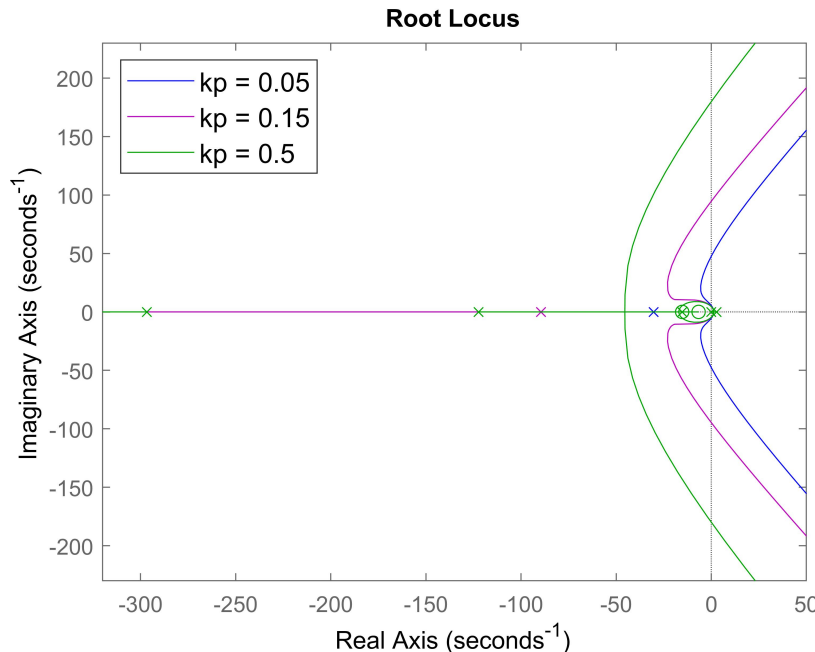


Figure 4.6 – Root locus of the system coupled to a PID controller ($T_d = 0.065$, $T_f = 0.008$ and $T_i = 0.150$).

A damping ratio of 0.7 is often chosen as a rule of good practice in control system because it allows a fast response while keeping a limited overshoot. Based on the root locus plotted on Figure 4.6, it appears that a low k_p such as 0.05 does not allow to obtain such damping ratio. Moreover, the higher k_p , the higher the gain margin of the outer loop. However, as previously discussed, the choice of k_p depends on the saturation of the motor current and requires considering the gearmotor backlash. Based on real device experiments, k_p has been chosen to be 0.15. Higher values of k_p induced aggressive gearmotor behaviour that

could wear the gear teethes over time. Using this value of k_p led to the following numerical transfer function (equation 4.8).

$$\frac{S(s)}{\omega_{sp}(s)} = \frac{112.4}{1.3s^3 + 132.7s^2 + 1407s - 4882} \quad (4.8)$$

Based on this numerical transfer function, the parameters of the PID controller have been calculated. Those are listed in Table 4.4.

T_d	0.150
T_f	0.065
T_i	0.008

Table 4.4 – Parameters of the PID controller for the centrifugal ring positioner.

The root locus of the transfer function 4.8 coupled with this PID controller is illustrated on Figure 4.7.

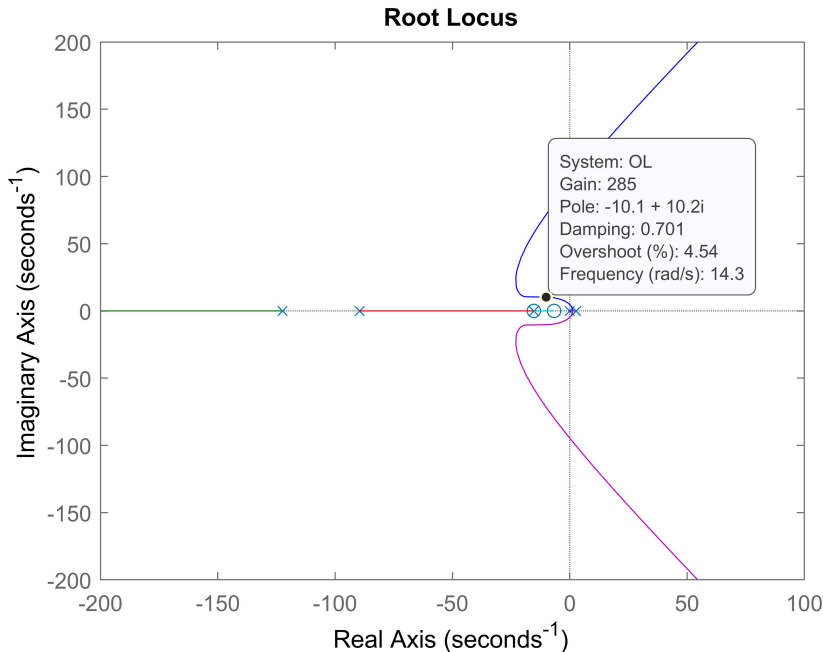


Figure 4.7 – Root locus of the system coupled to a PID controller ($T_d = 0.065$, $T_f = 0.008$ and $T_i = 0.150$) with $k_p = 0.15$.

Based on this root locus, the PID controller gain k has been chosen to be 285 in order to obtain a damping ratio of 0.701.

According to root locus analysis, such a gain leads to a stable closed-loop system in continuous-time case. It was then necessary to verify that the closed-loop would still be stable with such a gain when accounting for the sampling time and for the dead time due to the position measurement. To achieve that, Bode diagrams were used accounting for a dead time of 1 ms due to the numerical sampling⁴ and for a dead time of 16.5 ms due to the position sensor.

⁴The selection of the sampling period is discussed in the next section.

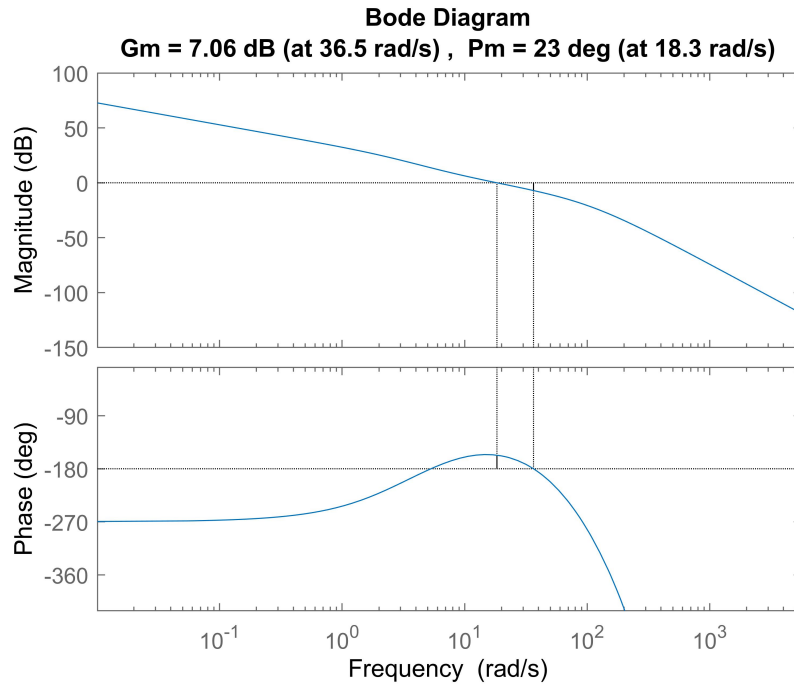


Figure 4.8 – Bode diagram of the centrifugal ring positioner coupled to a PID ($k = 285$, $T_d = 0.065$, $T_f = 0.008$ and $T_i = 0.150$).

As discussed in the control requirements, it was desired for the position control system to have a gain margin above 6 dB and a phase margin between 30° and 60° . For a gain of 285, these margins are showed on Figure 4.8. The gain margin is indeed above 6 dB but the phase margin is a little bit low. This is mainly due to the important dead time of the position sensor. One way to increase the phase margin is to lower the gain k , leading to a slower but more damped system dynamics. Changing the value of T_i also slightly influences the phase margin.

Even though the phase margin was lower than desired, this PID controller has been tested in simulation and then implemented on the microcontroller. Its transfer function is given by the equation 4.9.

$$D_s(s) = 285 \frac{(1 + 0.150s)}{0.150s} \frac{(1 + 0.065s)}{(1 + 0.008s)} \quad (4.9)$$

Discretization of the outer loop PID controller

Equation 4.9 corresponds to the transfer function of the PID controller in continuous-time. This had to be converted into a discrete transfer function to be implemented on the microcontroller. To achieve that, the Matlab instruction *c2d* has been used. Different discretization methods are available with this instruction such as Zero-Order Hold (ZOH), First-Order Hold (FOH), Tustin, Least-squares. Among them, the Tustin method is often used but since the ZOH method is the default one of the instruction *c2d*, it has been decided to investigate both methods. The best discretization method will be the one that leads to the closest results to the continuous controller results.

The discrete implementation of the controller requires the selection of a sampling period. As previously discussed, the design of the controllers was based on the conversion

of continuous transfer functions into discrete ones. It was therefore necessary to select small values of sampling period. For this reason, the sampling time T_s has been chosen to be 1 ms. However, it was also required to verify that this sampling period satisfied the Nyquist–Shannon sampling theorem. According to Bode diagrams, the bandwidth of the system coupled to the PID controller (equation 4.9) is about 38.5 rad/s. That means that the maximal frequency that needs to be sampled is about 6.1 Hz. According to this theorem, the sampling frequency must be at least equal to 12.2 Hz in order not to alter the measurements. The selected sampling frequency of 1000 Hz therefore widely satisfies the sampling theorem.

In order to investigate the best discretization method for the controller, simulated responses of the closed-loop linearised system between the ring position setpoint and the ring position have been plotted. These responses have been obtained by considering the inner loop previously designed as well as the outer loop PID controller in its continuous-time form and in each of its discretized forms. A input step change in the position setpoint leading to an important overshoot has been selected to better highlighting the differences between both discretization methods.

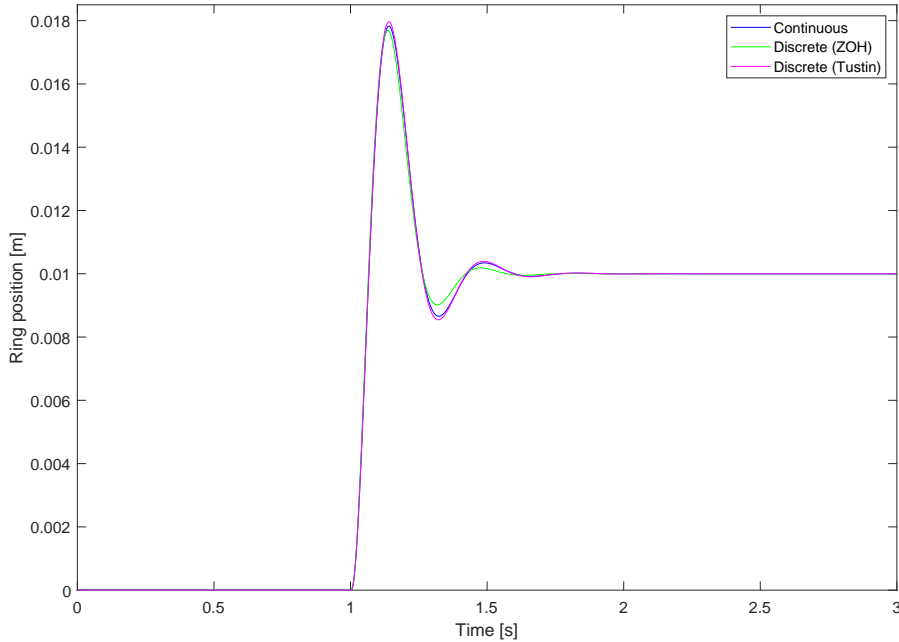


Figure 4.9 – Comparison of centrifugal ring positioner step responses for ZOH and Tustin discretization methods.

From Figure 4.9, it is clear that the Tustin method leads to a system step response more similar to the continuous controller than the one obtained with the ZOH. Moreover, when increasing the sampling time, the ZOH method leads to a larger discrepancy with the continuous-time closed-loop system compared to the Tustin method.

In addition to step responses analysis, Bode diagrams and stability margins have also been investigated. Figure 4.10 displays the Bode diagrams of each open loop while Table 4.5 contains their stability margins.

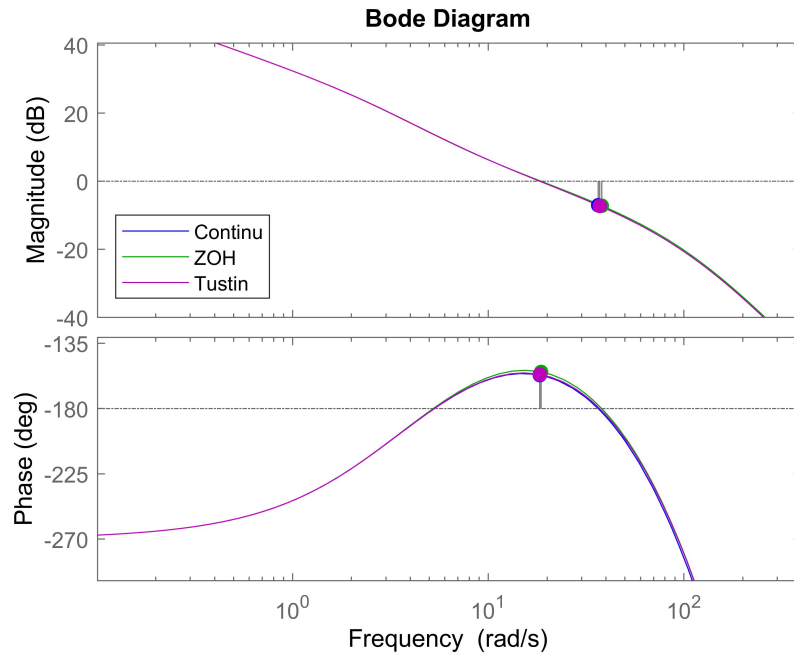


Figure 4.10 – Comparison of centrifugal ring positioner Bode diagrams for ZOH and Tustin discretization methods.

Controller	Gain margin	Phase margin
Continuous	7.06 dB	23.0°
ZOH	7.18 dB	25.2°
Tustin	7.26 dB	23.6°

Table 4.5 – Comparison of centrifugal ring positioner stability margins for ZOH and Tustin discretization methods.

As it can be observed on Figure 4.10, both discretization methods lead to very similar Bode diagrams. The stability margins are also relatively close to the continuous case. Again, increasing the sampling period increases the difference between the ZOH method and the continuous-time case, while this difference stays smaller for the Tustin method.

From this discussion, it appears that for a sampling period such small as 1 ms, both discretization methods could be used. The Tustin method seems leading to simulation results closer to the continuous-time case than the ZOH method. For this reason, the Tustin method has been chosen as discretization method for the digital implementation of the PID controller. The corresponding discrete transfer function is given by equation 4.10.

$$D_s(z) = \frac{2172z^2 - 4297z + 2125}{z^2 - 1.8850z + 0.8847} \quad (4.10)$$

All the control experiments that are further developed have also been performed with the ZOH digital controllers in order to observe if there exists significant differences with

the Tustin digital controllers. The results of the control of the centrifugal ring positioner with such controllers are given in Appendix C.

PID controlled outer loop simulation

This PID controller (equation 4.10) has been implemented in Simulink and different simulations have been conducted. With the aim of testing the performances of the controller on the centrifugal ring positioner, a specific ring position profile has been selected. It consisted of bringing the ring from its starting equilibrium position up to a determined higher position, to maintain it there for 5 s before progressively lowering it down to a position higher than the initial one. The resultant profile allowed to test the controller in up and down ring motions. The setpoint changes have been implemented as linear ramps and not as step changes to lower the risk of actuator saturation and to reduce sudden angular velocity variations, required to avoid backlash problems.

Figure 4.11 represents the evolution of the ring position, the motor angular velocity and the reference motor current during the simulation of the control problem.

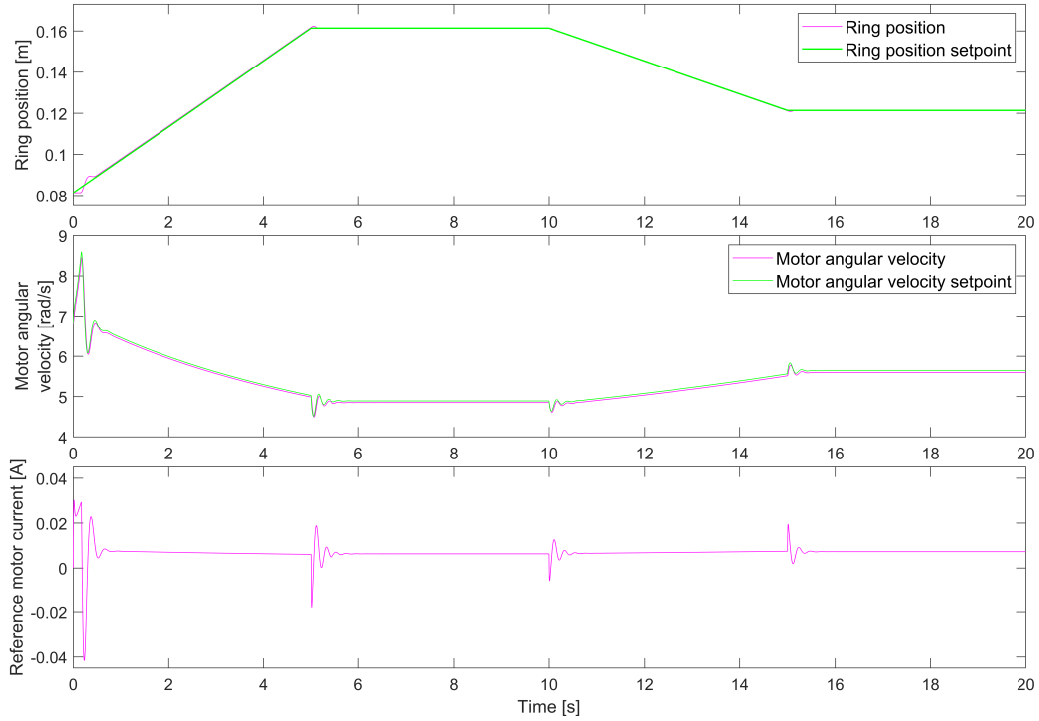


Figure 4.11 – Control simulation of the centrifugal ring positioner coupled to a PID controller ($k = 285$, $T_d = 0.065$, $T_f = 0.008$ and $T_i = 0.150$).

From this simulation, it resulted that this PID controller leads to a fast and precise setpoint tracking for the ring position. The position overshoot is limited thanks to the selected damping ratio coupled to a ramp setpoint change. As foreseen, the integrator part of the controller allows to follow the setpoint without steady-state error (for constant setpoint phases). Regarding the inner loop, the motor angular velocity follows properly its setpoint with a small offset due to the use of a simple P controller but this does not affect the ring position control performances. Thanks to the selected relatively low value of the

inner loop controller gain and to the ramp position setpoint change, sudden variations in the motor angular velocity setpoint are limited.

Implementation of the PID outer loop controller

The controller $D_s(s)$ that has been designed for the centrifugal ring positioner was based on a transfer function derived from the linearised system dynamics by considering a specific equilibrium point. Since the centrifugal ring positioner is an unstable system, it has to be brought close to this equilibrium point before being able to control the position with the controller. For this reason, an initialisation phase was implemented for the motor, consisting of a linear increase in the velocity setpoint from rest until the equilibrium velocity $\bar{\omega}$. The evolution of the motor velocity during this phase is represented on Figure 4.12.

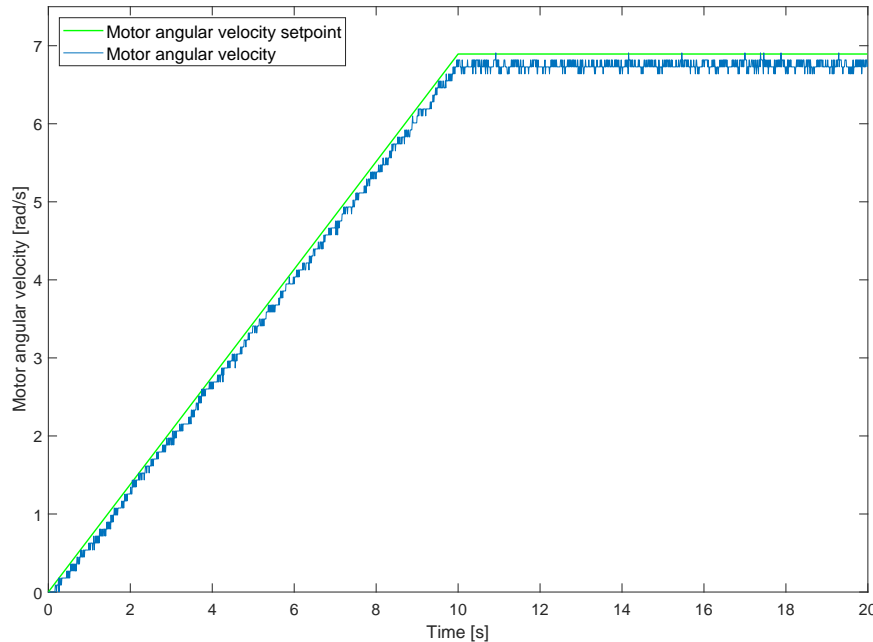


Figure 4.12 – Steering of the system from its rest position to the equilibrium point $(\bar{s}, \bar{\omega})$.

Once the motor reached the equilibrium point velocity, the control phase was started using the former PID controller (equation 4.10). The results of the control experiment are shown on Figure 4.13.

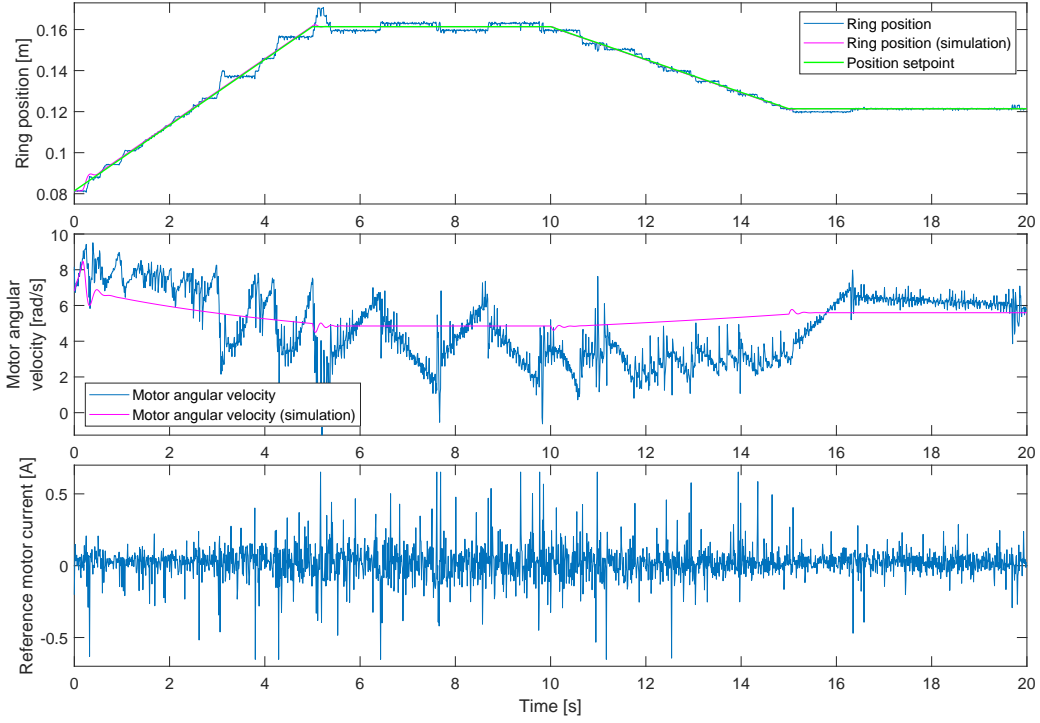


Figure 4.13 – Control of the centrifugal ring positioner coupled to a PID controller ($k = 285$, $T_d = 0.065$, $T_f = 0.008$ and $T_i = 0.150$).

From this experiment, it appeared that the designed PID controlled leads to proper set-point tracking for the ring position, mainly without significant offset. During the setpoint ramp phases, the presence of an offset higher than in simulation might be explained by rod imperfections making the ring not sliding homogeneously. For constant setpoint phases, the ring oscillates around its setpoint. These oscillations are explained by the integrator part of the controller coupled to friction phenomena. Indeed, as an illustration, let us consider what happened during the experiment after the first ramp overshoot occurring at $t \simeq 5$ s. At $t \simeq 5.5$ s, the ring was located slightly under its position setpoint. The controller thus acted to cancel this error by increasing the motor velocity but the ring was not able to move due to static friction. When the controller had sufficiently integrated the error, the angular velocity was that high so that the centrifugal force overcame the gravity and the static friction, making the ring sliding upwards. The ring was then located slightly higher than the setpoint and the situation was reversed, meaning now that the controller drove the motor velocity to decrease. This thus explains the roughly linear increases and decreases that are observed on the motor velocity graph. However, even though this controller led to proper control results, the variations of the reference motor current were relatively important, causing large sudden change in the motor angular velocity. As discussed previously, this behaviour should be avoided as much as possible.

To reduce these variations, a new PID controller based on two reflections has been implemented. First, it was assumed that the variations in the reference current and therefore in the motor angular velocity came from sudden fluctuations in the position sensor signal. Lowering the value of the filter coefficient N from 8 to 5 would thus allow to filter more the signal and lower these fluctuations. In addition to that, reducing the controller gain k

would make the controller less aggressive, leading to smaller current variations. The gain of the controller has therefore been reduced to 216, leading to a damping ratio of 0.54. The value of T_i has been changed from 0.15 to 0.16 to slightly increase the novel phase margin. The continuous transfer function of this newly designed controller is given by equation 4.11. The stability margin of this controller are 8.42 dB and 21.5°.

k	216
T_d	0.160
T_f	0.065
T_i	0.013

Table 4.6 – Parameters of the new PID controller for the centrifugal ring positioner.

$$D_s(s) = 216 \frac{(1 + 0.160s)}{0.160s} \frac{(1 + 0.065s)}{(1 + 0.013s)} \quad (4.11)$$

The corresponding discrete transfer function is given by equation 4.12

$$D_s(z) = \frac{1051z^2 - 2080z + 1029}{z^2 - 1.9260z + 0.9263} \quad (4.12)$$

The same control experiment than the one performed initially has been conducted with this controller. The results are shown on Figure 4.14.

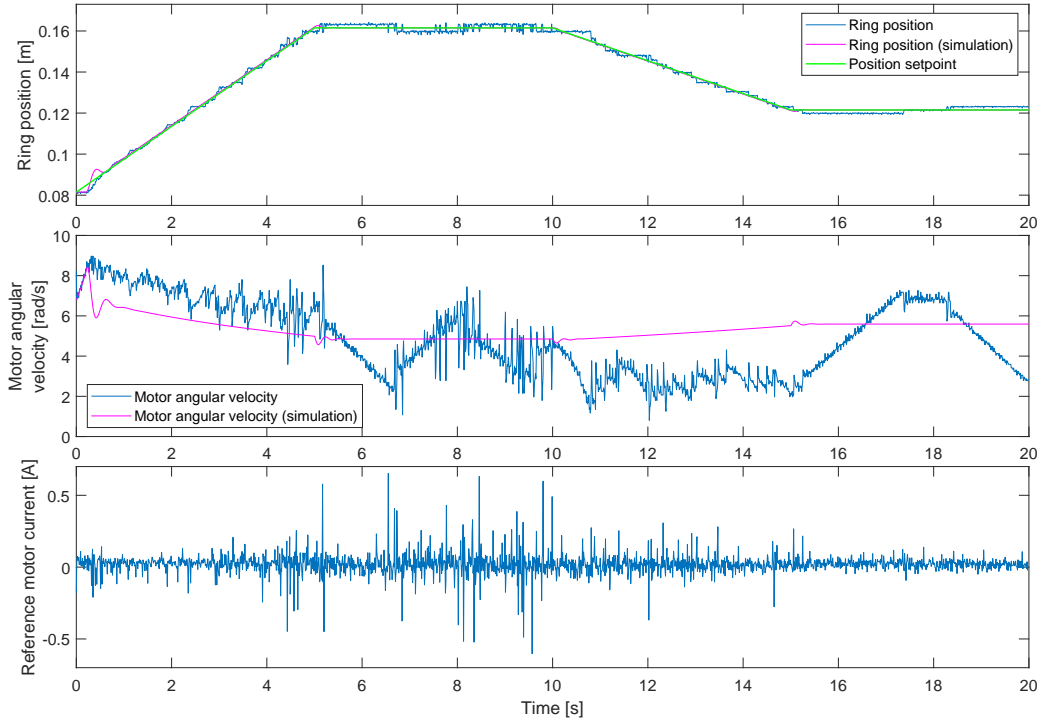


Figure 4.14 – Control of the centrifugal ring positioner coupled to a PID controller ($k = 216$, $T_d = 0.065$, $T_f = 0.013$ and $T_i = 0.160$).

Figure 4.14 shows that with this less aggressive PID controller, the centrifugal ring positioner still met the control requirement related to the ring position. The absence of

a significant overshoot could be observed due to the lower controller gain. Oscillations around the position setpoint were still present due to friction phenomena. Is it noteworthy to mention that these oscillations could be avoided by introducing a dead zone in front of the integrating action when the reference is constant. By opposition to the initial controller, sudden velocity variations were attenuated due to smaller reference current variations.

4.4.2 PD controller

Since both designed PID controllers led to a phase margin lower than the desired 30° , a PD controller has been investigated aiming at obtaining a more robust controlled system. However, it is noteworthy that since such a controller does not contain an integrator part, the ring position would not be able to follow its setpoint without offset.

Design of the outer loop PD controller

The transfer function of the considered PD controller is given by equation 4.13.

$$D_s(s) = k \frac{(1 + sT_d)}{(1 + sT_f)} \quad (4.13)$$

with $T_f = T_d/N$.

This controller presents 3 variable parameters, namely T_d , T_f and k . Like for the PID controller, the value of T_d has been chosen so that the corresponding controller zero cancels the first negative pole of the system. Based on the results of the PID controller experiments, the parameter N has directly been chosen to be 5. The gain k has been selected based on the root locus of equation 4.8 coupled with this PD controller.

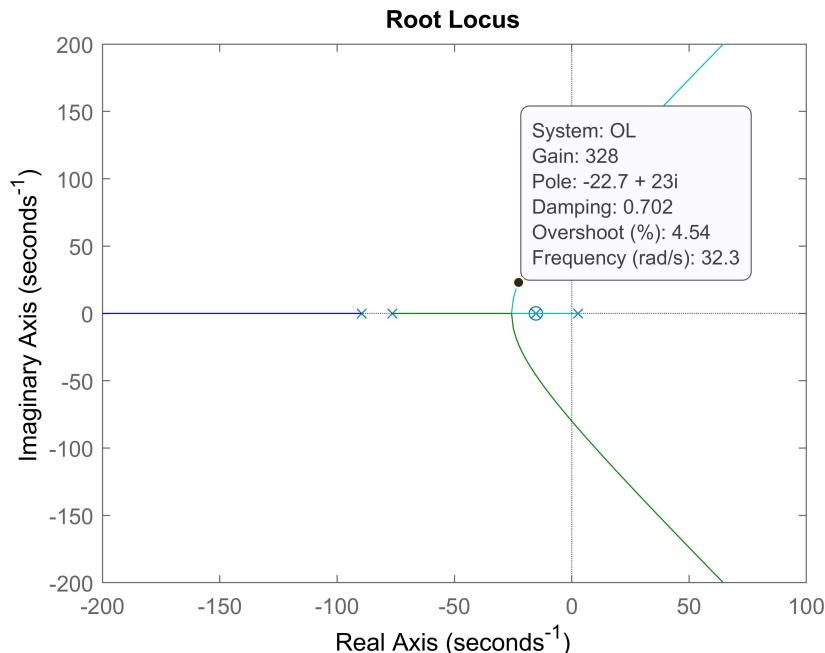


Figure 4.15 – Control of the centrifugal ring positioner coupled to a PD controller ($k = 328$, $T_d = 0.065$ and $T_f = 0.013$).

From Figure 4.15, a damping ratio of 0.702 results from a gain value of 328. According to Bode diagrams (Figure 4.16), such a gain leads to a gain margin of 6.71 dB and a phase margin of 36°. This phase margin is higher than both obtained with the PID controllers justifying thus the investigation of this PD controller.

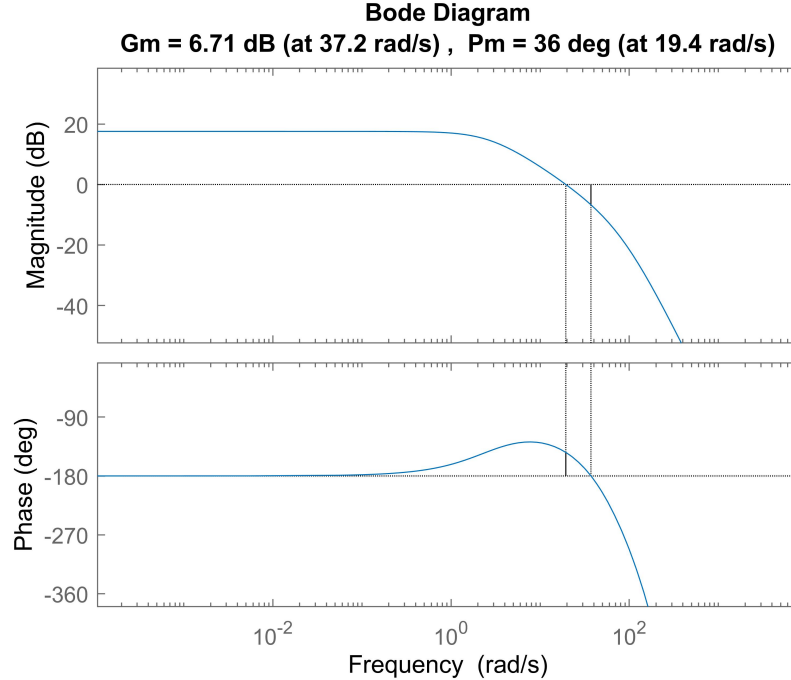


Figure 4.16 – Control of the centrifugal ring positioner coupled to a PD controller ($k = 328$, $T_d = 0.065$ and $T_f = 0.013$).

The numerical continuous transfer function of the PD controller is given by equation 4.14 and its discrete form is given by equation 4.15.

$$D_s(s) = 328 \frac{(1 + 0.065s)}{(1 + 0.013s)} \quad (4.14)$$

$$D_s(z) = \frac{1592z - 1568}{z - 0.9263} \quad (4.15)$$

PD controlled outer loop simulation

Like both PID controllers, the PD controller has been first implemented on Simulink. In order to compare controller performances, the same position setpoint profile has been selected. Figure 4.17 shows the results of the simulation.

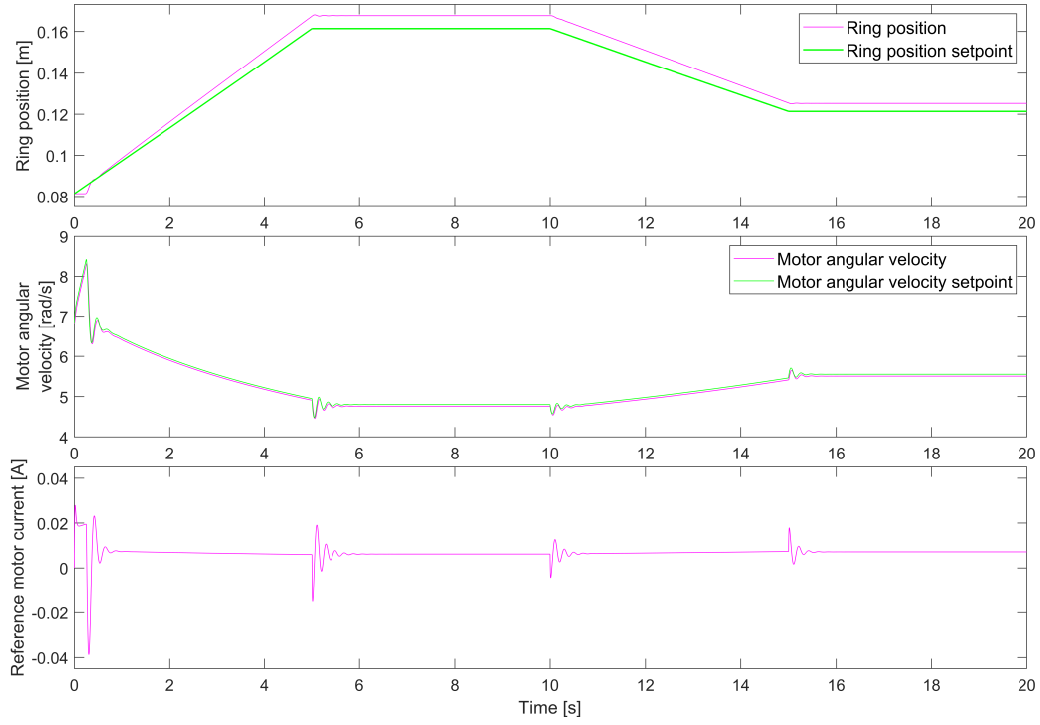


Figure 4.17 – Control simulation of the centrifugal ring positioner coupled to a PD controller ($k = 328$, $T_d = 0.065$ and $T_f = 0.013$).

Based on this simulation, the centrifugal ring positioner could be controlled with this PD controller. However, as expected, the absence of integrating action in the controller leads to a small position steady-state error with respect to its setpoint. This steady-state error could be lowered by increasing the controller gain. However, this would lower the gain margin under the desired 6 dB and would also lower the phase margin. Variations of the motor angular velocity and the reference current are similar to those encountered for the simulation of the system coupled with a PID controller (Figure 4.11).

Implementation of the outer loop PD controller

After conducting the simulation, the following step consisted in the implementation of the PD controller on the real device. The same initialisation phase, consisting of bringing the system close to its equilibrium point by increasing the motor angular velocity from rest was again performed. The results of the control experiment are represented on Figure 4.18.

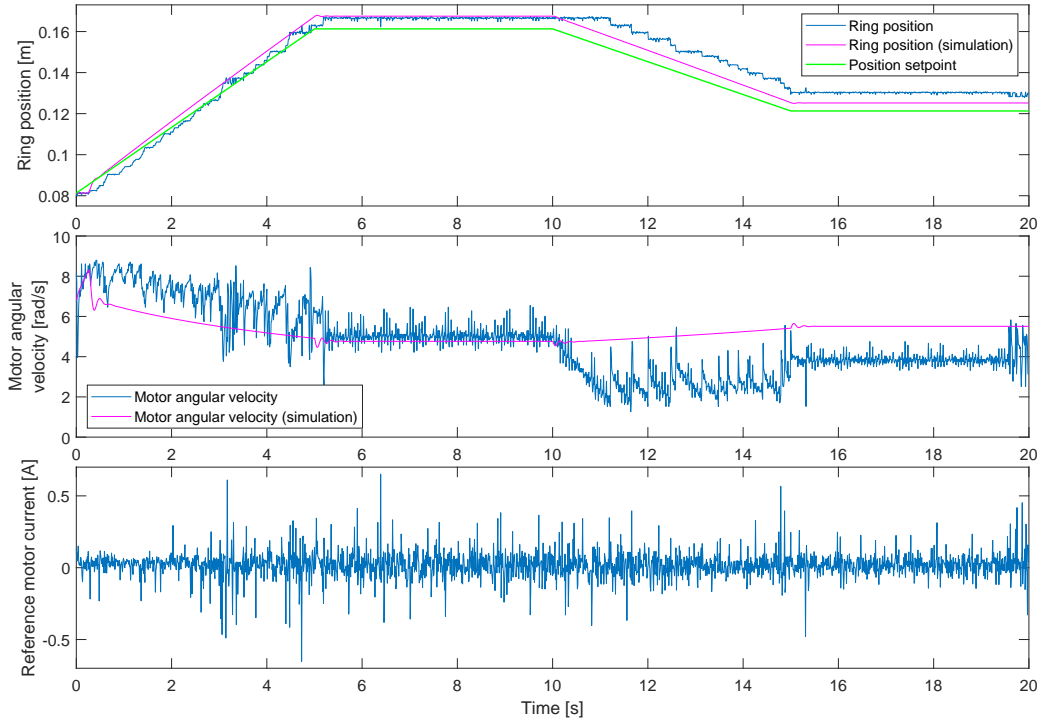


Figure 4.18 – Control of the centrifugal ring positioner coupled to a PD controller ($k = 328$, $T_d = 0.065$ and $T_f = 0.013$).

From the control experiment of the system with the PD controller, the ring followed its setpoint but with the expected presence of a steady-state error due to the absence of an integrating action in the controller. However, except for the negative ramp setpoint, the error between the ring position and its setpoint were quite limited, never exceeding 1 cm. Since there is no integrating action in the PD controller, the oscillating behaviour of the ring around its setpoint due to friction observed with the PID controllers did not take place in this case. This influenced also the motor velocity. As it can be seen on the motor angular velocity graph, the system presented a more homogeneous rotation than with PID controllers, where the velocity increased and decreased during constant setpoint phases in order to cancel the steady-state error. However, the reference motor current presented noticeable variations even though N was chosen to be 5. This caused backlash phenomena in the gear motor that could be heard during the experiment, leading therefore to gear teethes wear.

4.4.3 Comparison of outer loop controllers

Since both PID and PD controllers led to control of the ring position of the centrifugal ring positioner, it is interesting to compare them. The PID controller considered in this analysis is the second one, given by equation 4.11.

In terms of setpoint tracking, the PID controller led to much better results thanks to its integrating action cancelling the steady-state error between the ring position and its setpoint. We have seen that this integrating action had an influence on the motor angular velocity. Since the PD controller does not contain an integrating action, the system rotation

motion was more homogeneous with the PD controller than with the PID controller. The reference current showed less variations with the PID controller leading to lower gearmotor backlash phenomena, which is an important parameter to consider for the good working of the centrifugal ring positioner over time. It is also noteworthy that the steady-state error due to the use of a PD controller could have been lowered by increasing the controller gain. Keeping a gain margin above 6 dB would however have implied increasing the values of N , leading to even more backlash phenomena. This has therefore not been performed.

The main advantage of the PD controller compared to the PID controller is thus to present a higher phase margin, leading to more robustness. Even though its phase margin is lower than the desired 30° , it can be concluded that between both controllers, the PID is the most appropriate controller to control the ring position.

Chapter 5

Conclusion

The initial objective of the master thesis consisting in designing, building and controlling a centrifugal ring positioner has been properly achieved.

This non-linear benchmark has been inspired from an unstable device analysed in a project report of an Italian university. Since no additional relevant literature has been found about this device, the master thesis started with a state of the art which aimed at identifying similarities and differences between the centrifugal ring positioner and well-known control system benchmarks such as the inverted pendulum and the ball and beam. Specifically, the control of each system by cascade control strategy was highlighted. Moreover, sensors used in such benchmarks have orientated the selection of the sensors for the centrifugal ring positioner.

The development of the mathematical modelling of the system dynamics has then been performed applying the second Newton's law of motion and the angular momentum theorem. This resulted in a non-linear system of equations that has been linearised around an equilibrium point, leading to a state-space representation of the centrifugal ring positioner.

Taking into account the rare literature about the system, keeping its design as simple as possible was a key element to consider for the design of the centrifugal ring positioner. Hence, we opted for the present design of the system, consisting of a 3D-printed PLA ring sliding on an aluminium rod. Regarding the components, an Arduino DUE has been selected as controller device. The actuator of the system consists of a DC gearmotor coupled to a motor driver. An infrared sensor has been selected for monitoring the ring position and an incremental encoder has been used for measuring the motor angular velocity.

The first control requirement of the centrifugal ring positioner has been defined as ring position setpoint tracking while the second requirements regards the system robustness. Gain margins above 6 dB and phase margin between 30° and 60° were desired. To achieve these requirements, cascade control inspired by the ball and beam reported in the state of the art has been implemented. The gearmotor was considered as the inner subsystem while the outer one consisted in the motor angular velocity-ring position system. A transfer function for the inner subsystem was derived through a black-box experiment in order to obtain a realistic model of the loaded motor. The motor has been controlled by a P controller to lower as much as possible the effect of friction disturbances. Different values of the controller gain have been tested, all leading to satisfactory results in simulation and on the real device. The final choice of the controller gain was performed during the design of the outer loop controller, accounting for actuator saturation and for gearmotor backlash. Two controllers have been designed and tested for controlling the ring position. A PID controller has first been designed since it would allow to cancel any steady-state error between the ring position and its setpoint. Some modifications such a lowering the gain and increasing the filtering part have been performed on the controller in order to make it less aggressive and to reduce gear teethes wear over time.

Since the phase margin of this PID was lower than the desired 30° specified by the second requirement, a PD controller has also been designed for the outer loop aiming at obtaining a more robust controlled system. Both controllers allowed to meet the first control specification. However, despite its resulting lower phase margin, the PID has appeared to be a more appropriate controller for the centrifugal ring positioner. Indeed, it allowed the ring to track its setpoint with limited offset (due to friction phenomena), this offset being way higher for the PD controller. Moreover, the reference current showed less variations for the PID controller than for the PD controller, leading to less gearmotor backlash.

From a pedagogical point of view, the centrifugal ring positioner designed in this master thesis is an interesting didactic device allowing to illustrate the cascade control of an unstable and non-linear system. It presents several advantages compared to existing benchmarks such as the cart inverted pendulum or the ball and beam. First, the centrifugal ring positioner is a very simple device to build since most of its pieces can be 3D-printed implying an overall relatively low cost. Indeed, its total cost has been estimated to be less than 1000€, with the major part coming from the Maxon components (gearmotor, motor driver and encoder). As such, it consists of a quite easily reproducible device. Moreover, the centrifugal ring positioner presents a very compact design still allowing to obtain good control theory concepts illustrations. By opposition, it is quite complicated to build a compact inverted pendulum without setting aside its impressive upswing phase. In term of compactness, the centrifugal ring positioner is closer to the ball and beam. It presents however a more reliable position measurement than the ball and beam of the SAAS department, both using the same position sensor. Indeed, the ball of the SAAS ball and beam degrades with time by hitting the rubber stop at the end of the beam. This causes dark spots on it affecting the position measurements. Moreover, the plane surface of the ring allows a better measurement of the mobile position than the spherical shape of the ball. The only question mark concerning the centrifugal ring positioner ageing is the ring wear. We don't know yet how it will deteriorate with time and how that will affect its friction on the rod. 3D-printing materials with lower friction coefficient and therefore leading to less ring deterioration such as *Igus* 3D-printing materials^[41] could be envisaged. In any cases, printing a new ring when the current one is worn is very fast and cheap. Based on the slip ring and gearmotor lifetime reported by their manufacturers, the centrifugal ring positioner should be operational for control systems labs for decades. The gear teethes wear of the gearmotor will however be an important element to consider for the ageing of the centrifugal ring positioner. Finally, it is noteworthy to mention a non-negligible drawback of the centrifugal ring positioner being that the system is rotating, which might be dangerous in case of lack attention by the students. This potential hazard could be overcome by adding a transparent Poly-Vinyl Chloride (PVC) box around the system. On a material safety point of view, the centrifugal ring positioner does not have any mechanical stop hindering the motor rotation like for example cart end rails stops in the inverted pendulum. The motor can therefore not be burned and the stops can thus not be broken.

Although the centrifugal ring positioner has been fully designed and properly controlled in the framework of this master thesis, this work has also allowed to identify potential improvement areas such as:

- The design of the system, mainly of the mobile and the rod, as well as their materials

could be challenged in order to reduce non-homogeneous friction effects. Replacing the rod by another one with a better surface finish would already be a promising improvement.

- The design of the rod coupling piece could also be readdressed in order to obtain a system with a modifiable rod angle. This would lead to a more challenging control of the ring position.
- The oscillations of the ring around its setpoint due the static friction phenomena observed when the PID controller was used could be cancelled by improving the integrating part of the controller, by introducing a dead zone in the integrating action when the position reference is constant.
- The gearmotor could be replaced by another motor, without reduction gear.
- Others control strategies than cascade control as well as other controller types could be investigated for the control of the centrifugal ring positioner.
- With small modifications, the rotating base of the centrifugal ring positioner (gearmotor + encoder + slip ring) might be suitable for the design of a rotary inverted pendulum. One could therefore imagine a system with a common rotating base, being able to host either the tilted arm of the centrifugal ring positioner or the pendulum rod of a rotary inverted pendulum. This modular conception would thus lead to a twofold purpose didactic device.

Bibliography

- [1] Lee J, Mukherjee R, Khalil HK. Output feedback stabilization of inverted pendulum on a cart in the presence of uncertainties. *Automatica*. 2015 Apr;54:146–157.
- [2] Seborg DE. Process Dynamics and Control. 3rd ed. Hoboken, N.J.: John Wiley & Sons; 2011.
- [3] Peker F, Kaya I, Cokmez E, Atic S. Cascade Control Approach for a Cart Inverted Pendulum System Using Controller Synthesis Method. In: 2018 26th Mediterranean Conference on Control and Automation (MED). Zadar, Croatia: IEEE; 2018. p. 1–6.
- [4] Acharya M, Bhattacharai M, Poudel B. Real Time Motion Assessment for Positioning In Time and Space Critical Systems. *International Journal of Applied Research and Studies*. 2014;3(7):12.
- [5] Lv XH, Liu YX, Liu Y, Huang HY. Design of Ball-Beam Control System Based on Machine Vision. *Applied Mechanics and Materials*. 2011 Jul;71-78:4219–4225.
- [6] Famularo D, Fortuna A. Project Report: Tecniche Di Controllo Ottimo Applicate Ad Un Sistema Meccanico. Facolta Di Ingegneria Univerista Della Calabria;.
- [7] Arduino Due, Arduino Official Store;. Available from: <https://store.arduino.cc/arduino-due>.
- [8] Maxon 118746 DC motor with gearbox;. Available from: https://www.toolex.com/index.php?route=product/product&product_id=2323.
- [9] ESCON 50/5 Documentation Hardware. 2015;p. 40.
- [10] Maxon Online Shop, Maxon Group;. Available from: <https://www.maxongroup.com/maxon/view/product/110515>.
- [11] H2056 Series Mini Through Hole Slip Ring, Senring;. Available from: <https://www.senring.com/through-hole-slip-ring/h2056.html>.
- [12] Motor M. High Precision Drives and Systems, Program 2019/2020; 2019.
- [13] Sharp. Sharp GP2Y0A41SK0F Datasheet;.
- [14] HC-SR04 Datasheet;.
- [15] MT2042 series Rotary Slip Ring, Moflon;. Available from: <https://www.moflon.com/mt2042.html>.
- [16] Bencomo SD. Control Learning: Present and Future. *IFAC Proceedings Volumes*. 2002;35:71–93.
- [17] Kawlewska K, Watroba P. Design of an inverted pendulum laboratory stand to teach mechatronics. Yogyakarta, Indonesia; 2018. p. 020027.
- [18] Boubaker O. The Inverted Pendulum Benchmark in Nonlinear Control Theory: A Survey. *International Journal of Advanced Robotic Systems*. 2013 May;10(5):233.

- [19] Horacek P. Laboratory Experiments For Control Theory Courses: A Survey. 2000;p. 12.
- [20] Kheir NA, Åström KJ, Auslander D, Cheok KC, Franklin GF, Masten M, et al. Control systems engineering education. *Automatica*. 1996 Feb;32(2):147–166.
- [21] Irfan S, Mehmood A, Razzaq MT, Iqbal J. Advanced sliding mode control techniques for Inverted Pendulum: Modelling and simulation. *Engineering Science and Technology, an International Journal*. 2018 Aug;21(4):753–759.
- [22] Magdy M, El Marhomy A, Attia MA. Modeling of inverted pendulum system with gravitational search algorithm optimized controller. *Ain Shams Engineering Journal*. 2019 Mar;10(1):129–149.
- [23] Prasad LB, Tyagi B, Gupta HO. Optimal Control of Nonlinear Inverted Pendulum System Using PID Controller and LQR: Performance Analysis Without and With Disturbance Input. *International Journal of Automation and Computing*. 2014 Dec;11(6):661–670.
- [24] Wang JJ. Simulation studies of inverted pendulum based on PID controllers. *Simulation Modelling Practice and Theory*. 2011 Jan;19(1):440–449.
- [25] Yurkovich S, Widjaja M. Fuzzy controller synthesis for an inverted pendulum system. *Control Engineering Practice*. 1996 Apr;4(4):455–469.
- [26] Oltean SE. Swing-up and Stabilization of the Rotational Inverted Pendulum Using PD and Fuzzy-PD Controllers. *Procedia Technology*. 2014;12:57–64.
- [27] Bitirgen R, Hancer M, Bayezit I. All Stabilizing State Feedback Controller for Inverted Pendulum Mechanism. *IFAC-PapersOnLine*. 2018;51(4):346–351.
- [28] Ponce. A Review Of Intelligent Control Systems Applied To The Inverted-Pendulum Problem. *American Journal of Engineering and Applied Sciences*. 2014 Feb;7(2):194–240.
- [29] Guinaldo M, Vargas H, Sánchez J, Sanz E, Dormido S. Web-based Control Laboratory: The Ball and Beam System. *IFAC Proceedings Volumes*. 2010;42(24):174–179.
- [30] Oh SK, Jang HJ, Pedrycz W. Optimized fuzzy PD cascade controller: A comparative analysis and design. *Simulation Modelling Practice and Theory*. 2011 Jan;19(1):181–195.
- [31] Middleton RH, Goodwin GC. Digital control and estimation: a unified approach. Englewood Cliffs: Prentice-Hall; 1990.
- [32] Inc Q. Quanser Inverted Pendulum IP02 User Manual; 2012.
- [33] Soumelidis A, Gáspár P, Bokor J. Inverted Pendulum: An Environment for Intelligent Control Design and Test. *IFAC Proceedings Volumes*. 1997 Jun;30(7):381–385.
- [34] Saad M, Khalallah M. Design and Implementation of an Embedded Ball-beam Controller Using PID Algorithm. *Universal Journal of Control and Automation*. 2017;p. 8.

- [35] Mehedi IM, Al-Saggaf UM, Mansouri R, Bettayeb M. Two degrees of freedom fractional controller design: Application to the ball and beam system. *Measurement*. 2019 Mar;135:13–22.
- [36] Choudhary MK, Kumar GN. ESO Based LQR Controller for Ball and Beam System. *IFAC-PapersOnLine*. 2016;49(1):607–610.
- [37] Meenakshipriya B, Kalpana K. Modelling and Control of Ball and Beam System using Coefficient Diagram Method (CDM) based PID controller. *IFAC Proceedings Volumes*. 2014;47(1):620–626.
- [38] Taifour Ali A, A M A, H A A, A Taha O, Naseraldeen A A. Design and Implementation of Ball and Beam System Using PID Controller. *Automatic Control and Information Sciences*. 2017 Aug;3(1):1–4.
- [39] Inc Q. Quanser Ball and Beam BB01 User Manuel; 2011.
- [40] Lambert P. Mécanique Rationnelle II: MECA-H200. Bruxelles: Presses universitaires de Bruxelles (PUB); 2019.
- [41] 3D printing materials | igus®;. Available from: <https://www.igus.hr/3d-print-material/3d-print-material>.
- [42] Franklin G, Powell JD. Digital Control of Dynamic Systems. Addison-Wesley Publishing Company; 1980.

Appendix A

Inertia tensor of the CRP

To calculate the inertia of the centrifugal ring positioner, it is more convenient to decompose the system in several pieces, namely A, B, C, D, E and F (Figure A.1). The inertia tensor is calculated in the XYZ axes. Note that in Section 2.2, we noticed that only the element j_{33} of the complete tensor of inertia is needed for the mathematical development of the system dynamics. Therefore for each piece, only the element j_{33} is needed and it is therefore not necessary to calculate the overall inertia tensor.

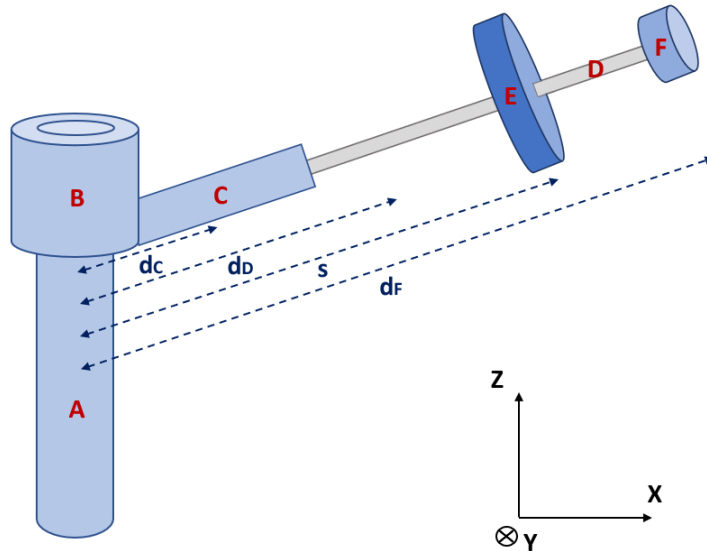


Figure A.1 – Simplified representation of the centrifugal ring positioner and decomposition in pieces for the inertia tensor calculation.

Table A.1 contains the assumed shape for each piece of the system as well as the different dimension parameters that are involved in the inertia calculations.

	Shape	Dimensions
Piece A	Full cylinder	Radius: R_A
Piece B	Hollow cylinder	External radius: $R_{B,ext}$ Internal radius: $R_{B,int}$
Piece C	Parallelepiped rectangle	Length: L_C Width: W_C Height: H_C
Piece D	Full cylinder	Radius: R_D Length: L_D
Piece E	Full cylinder	Radius: R_E Length: L_E
Piece F	Full cylinder	Radius: R_F Length: L_F

Table A.1 – Pieces constituting the centrifugal ring positioner for the calculation of the tensor of inertia.

Based on the shapes, the following tensors of inertia can be calculated [40].

$$J_A = \begin{pmatrix} / & / & / \\ / & / & / \\ / & / & \frac{m_A}{2} R_A^2 \end{pmatrix} \quad J_B = \begin{pmatrix} / & / & / \\ / & / & / \\ / & / & \frac{m_B}{2} (R_{B,int}^2 + R_{B,ext}^2) \end{pmatrix}$$

$$J_C = \begin{pmatrix} / & / & / \\ / & / & / \\ / & / & \frac{m_C}{12} (W_C^2 + H_C^2) \sin^2 \theta + \left(\frac{m_C}{12} (W_C^2 + L_C^2) + m d_C^2 \right) \cos^2 \theta \end{pmatrix}$$

$$J_D = \begin{pmatrix} / & / & / \\ / & / & / \\ / & / & \frac{m_D}{2} R_D^2 \sin^2 \theta + \left(\frac{m_D}{4} (R_D^2 + \frac{L_D^2}{3}) + m d_D^2 \right) \cos^2 \theta \end{pmatrix}$$

$$J_E = \begin{pmatrix} / & / & / \\ / & / & / \\ / & / & \frac{m_E}{2} R_E^2 \sin^2 \theta + \left(\frac{m_E}{4} (R_E^2 + \frac{L_E^2}{3}) + m s^2 \right) \cos^2 \theta \end{pmatrix}$$

$$J_F = \begin{pmatrix} / & / & / \\ / & / & / \\ / & / & \frac{m_F}{2} R_F^2 \sin^2 \theta + \left(\frac{m_F}{4} (R_F^2 + \frac{L_F^2}{3}) + m d_F^2 \right) \cos^2 \theta \end{pmatrix}$$

All the inertia tensor elements $_{33}$ are constant except the one of the mobile (piece E). Indeed, since the mobile can move, its distance with the rotational axis can vary. The tensor of inertia of the overall system is given by the sum of each tensor part.

$$J = J_A + J_B + J_C + J_D + J_E + J_F = \begin{pmatrix} / & / & / \\ / & / & / \\ / & / & j_{33} \end{pmatrix} = \begin{pmatrix} / & / & / \\ / & / & / \\ / & / & i_{33} + m s^2 \cos^2 \theta \end{pmatrix}$$

with

$$\begin{aligned} i_{33} = & \frac{m_A}{2} R_A^2 + \frac{m_B}{2} (R_{B,int}^2 + R_{B,ext}^2) + \frac{m_C}{12} (W_C^2 + H_C^2) \sin^2 \theta \\ & + \left(\frac{m_C}{12} (W_C^2 + L_C^2) + m d_C^2 \right) \cos^2 \theta + \frac{m_D}{2} R_D^2 \sin^2 \theta + \left(\frac{m_D}{4} (R_D^2 + \frac{L_D^2}{3}) + m d_D^2 \right) \cos^2 \theta \\ & + \frac{m_E}{2} R_E^2 \sin^2 \theta + \frac{m_E}{4} (R_E^2 + \frac{L_E^2}{3}) \cos^2 \theta + \frac{m_F}{2} R_F^2 \sin^2 \theta + \left(\frac{m_F}{4} (R_F^2 + \frac{L_F^2}{3}) + m d_F^2 \right) \cos^2 \theta \end{aligned}$$

Appendix B

Ring viscous friction coefficient

The numerical value of the viscous friction coefficient of the ring on the rod is required for the control of the centrifugal ring positioner since it is involved in simulations and in controllers design. Various tables exist containing friction coefficient data between two materials but data for PLA on aluminium are however not available. For this reason, the value of this coefficient has been determined through an experiment.

The principle of the experiment was to monitor the evolution of the ring position with time when increasing the motor angular velocity. Starting from the equilibrium point ($\bar{s} = 0.08 \text{ m}$, $\bar{\omega} = 6.89 \text{ rad/s}$), the motor angular velocity was progressively increased in order to make the ring slide from its rest position towards the end of the rod. Then, the ring position evolution was compared to simulations based on the non-linear system dynamics derived in Section 2.2 and on the identified motor transfer function. Different values of viscous friction coefficient have been tested in simulation in order to fit as well as possible to the experimental data. It has been found that the ring viscous coefficient was about 0.3 kg/s . The experimental data as well as the corresponding simulation are illustrated on Figure B.1. This experiment also allowed to approximate a value for the static friction force opposed to the ring motion. This force, found to be around 0.04 N , was used in simulation to obtain a more realistic model of the system dynamics.

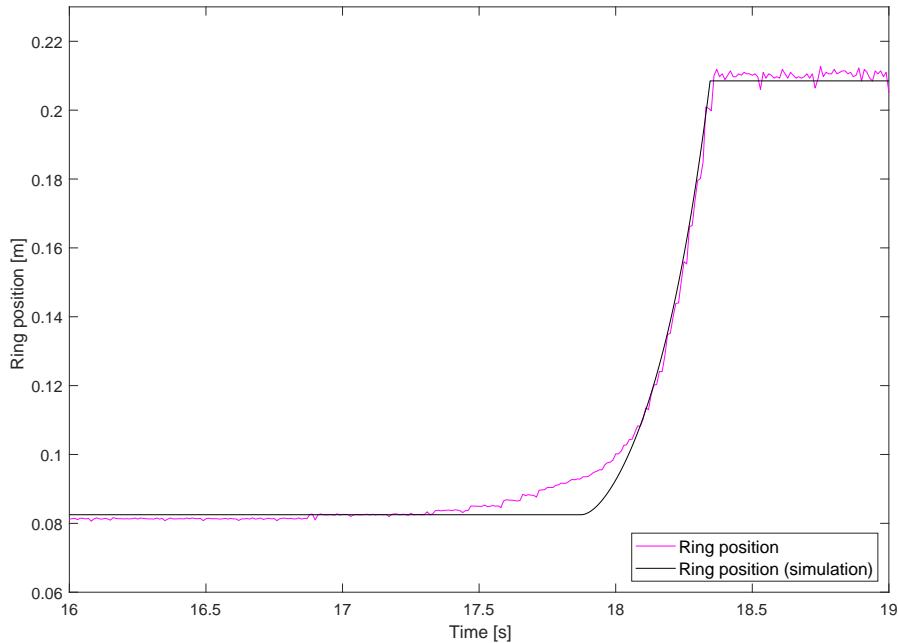


Figure B.1 – Experimental determination of the ring viscous friction coefficient.

A difference between the experimental data and the simulation was observed at the beginning of the ring motion. This is probably caused by the fact that the rod presents some significant imperfections on the first 1.5 cm, altering the proper sliding of the ring.

Appendix C

Zero-Order Hold discretization method

The Zero-Order Hold (ZOH) method is a discretization method based on the assumption that the input signal (the control error) is constant over the sampling period. It is therefore intuitive that the lower the sampling period, the better the discrete approximation of the continuous signal^[42]. As discussed in Section 4.4.1, this method, such as the Tustin method, seems leading to simulation results very close to the ones obtained with the continuous-time controller for a sampling period of 1 ms. For this reason, the same three control experiments that have been performed in Section 4 have been reproduced by implementing digital controllers discretized by the ZOH method. The aim is to observe if the results significantly differ from the ones obtained with the Tustin method.

The ZOH discrete transfer function of the first PID controller (equation 4.9) is given by equation C.1.

$$D_s(z) = \frac{2280z^2 - 4513z + 2233}{z^2 - 1.8850z + 0.8848} \quad (\text{C.1})$$

Figure C.1 shows the experimental results obtained with such controller.

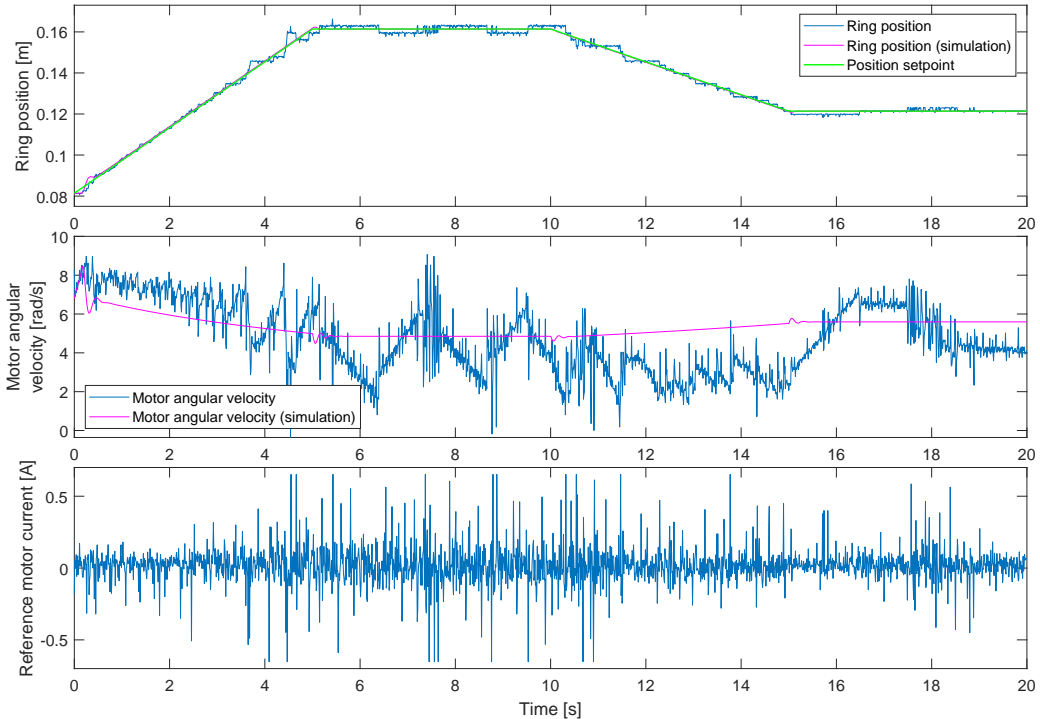


Figure C.1 – Control of the centrifugal ring positioner coupled with a PID controller ($k = 285$, $T_d = 0.065$, $T_f = 0.008$ and $T_i = 0.150$) using ZOH discretization method.

Like the first PID controller, the continuous transfer function of the second PID controller (equation 4.11) has been converted into a discrete one using the ZOH method, resulting in equation C.2. The resulting control results of the system are represented on Figure C.2.

$$D_s(z) = \frac{1080z^2 - 2138z + 1058}{z^2 - 1.9260z + 0.9264} \quad (\text{C.2})$$

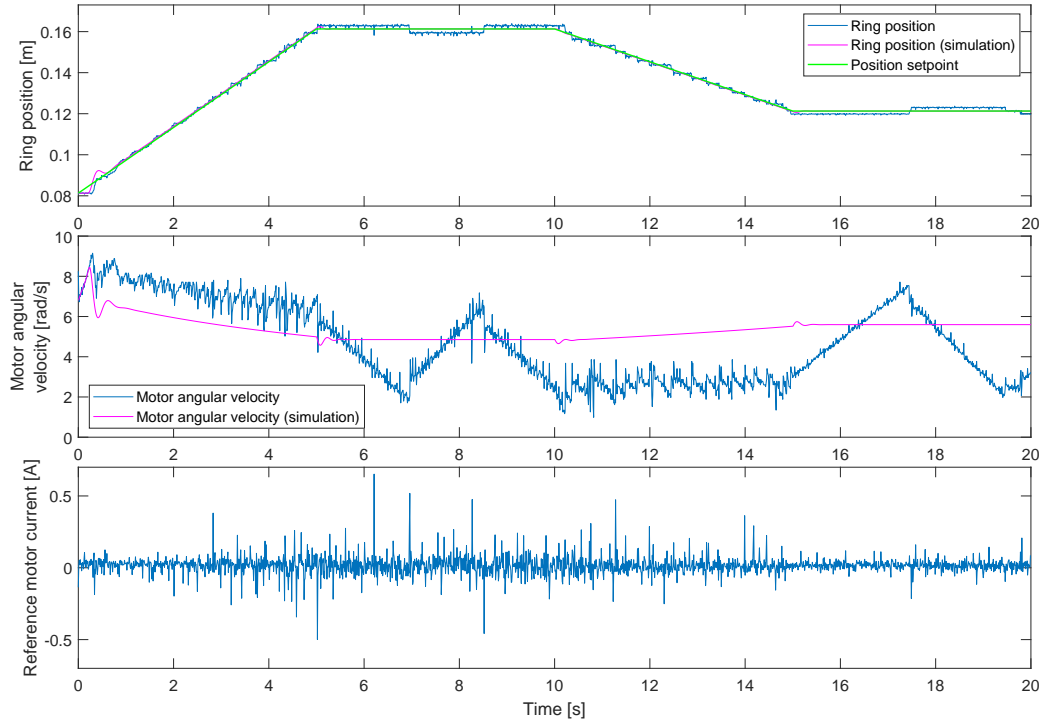


Figure C.2 – Control of the centrifugal ring positioner coupled with a PID controller ($k = 216$, $T_d = 0.065$, $T_f = 0.013$ and $T_i = 0.160$) using ZOH discretization method.

Finally, the PD controller (equation 4.14) has also been converted via the ZOH method, leading to equation C.3 and to the results illustrated on Figure C.3.

$$D_s(z) = \frac{1640z - 1616}{z - 0.9264} \quad (\text{C.3})$$

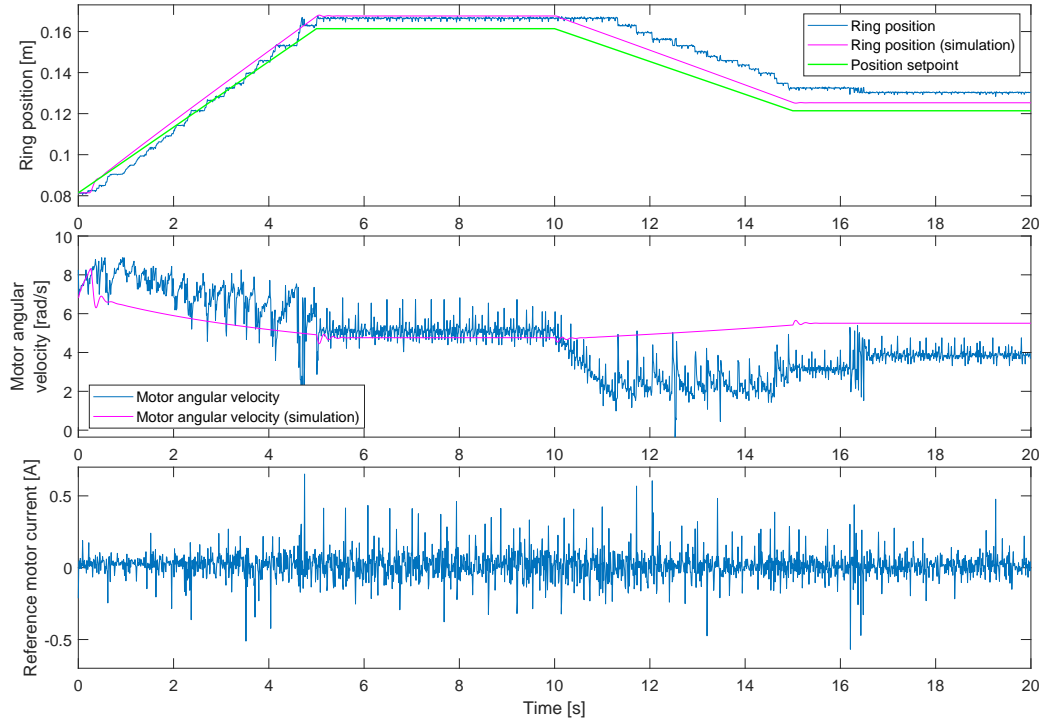


Figure C.3 – Control of the centrifugal ring positioner coupled with a PD controller ($k = 328$, $T_d = 0.065$ and $T_f = 0.013$) using ZOH discretization method.

For the three experiments, the obtained results are very similar to the ones obtained with the Tustin discretized controllers. This could be predicted since each controller discrete transfer function is really similar to the corresponding transfer function obtained with the Tustin discretization method. These transfer functions similarities are explained by the high sampling frequency of 1000 Hz. Decreasing this sampling frequency increases the differences between the controllers transfer functions obtained with each discretization method. One could therefore expect that a higher difference between the experimental results obtained with each discretized would exist if the sampling frequency was lower.

Appendix D

Simulink model of the CRP

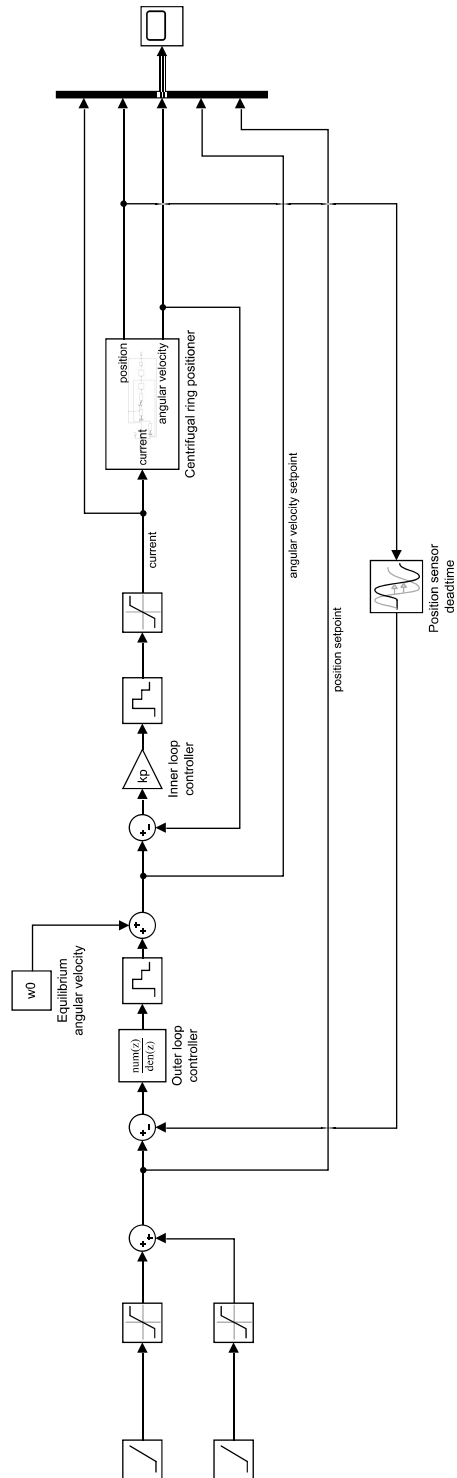


Figure D.1 – Simulink model of the cascade control of the centrifugal ring positioner.

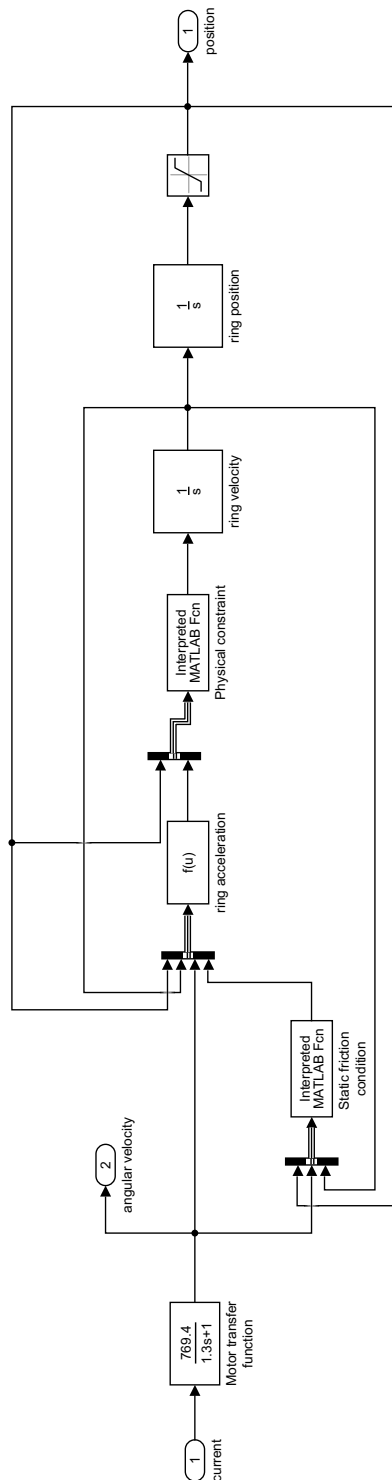


Figure D.2 – Simulink model of the centrifugal ring positioner.